A HIGH-RESOLUTION AND OBSERVATIONALLY CONSTRAINED OMI NO_2 SATELLITE RETRIEVAL

Daniel L. Goldberg*[,1,2], Lok N. Lamsal [3,4], Christopher P. Loughner [5,6], William H. Swartz[4,7], Zifeng Lu [1,2], and David G. Streets [1,2]

[1]Energy Systems Division, Argonne National Laboratory, Argonne, IL 60439, USA

[2]Computation Institute, University of Chicago, Chicago, IL 60637, USA

[3]Goddard Earth Sciences Technology and Research, Universities Space Research Association, Columbia, MD 21046, USA

[4]NASA Goddard Space Flight Center, Code 614, Greenbelt, MD 20771, USA

[5]NOAA Air Resources Laboratory, College Park, MD 20740, USA

[6]Earth System Science Interdisciplinary Center, University of Maryland, College Park, MD 20740, USA

[7]Johns Hopkins University Applied Physics Laboratory, Laurel, MD 20723, USA

Paper submitted to

Atmospheric Chemistry and Physics

Originally submitted: March 9, 2017
Revised draft submitted: August 21, 2017

*Corresponding author. Phone: (630) 252-3931; Fax: (630) 252-8007; Email: dgoldberg@anl.gov.

A high-resolution and observationally constrained OMI NO_2 satellite retrieval

Daniel L. Goldberg[1,2], Lok N. Lamsal[3,4], Christopher P. Loughner[5,6], William H. Swartz[4,7], Zifeng Lu[1,2], and David G. Streets[1,2]

[1]Energy Systems Division, Argonne National Laboratory, Argonne, IL 60439, USA
[2]Computation Institute, University of Chicago, Chicago, IL 60637, USA
[3]Goddard Earth Sciences Technology and Research, Universities Space Research Association, Columbia, MD 21046, USA
[4]NASA Goddard Space Flight Center, Code 614, Greenbelt, MD 20771, USA
[5]NOAA Air Resources Laboratory, College Park, MD 20740, USA
[6]Earth System Science Interdisciplinary Center, University of Maryland, College Park, MD 20740, USA
[7]Johns Hopkins University Applied Physics Laboratory, Laurel, MD 20723, USA

Correspondence to: Daniel L. Goldberg (dgoldberg@anl.gov)

Abstract. This work presents a new high-resolution NO_2 dataset derived from the NASA Ozone Monitoring Instrument (OMI) NO_2 version 3.0 retrieval that can be used to estimate surface level concentrations. The standard NASA product uses NO_2 vertical profile shape factors from a 1.25° × 1° (~110 × 110 km) resolution Global Model Initiative (GMI) model simulation to calculate air mass factors, a critical value used to determine observed tropospheric NO_2 vertical columns. To better estimate vertical profile shape factors, we use a high-resolution (1.33 × 1.33 km) Community Multi-scale Air Quality (CMAQ) model simulation constrained by in situ aircraft observations to re-calculate tropospheric air mass factors and tropospheric NO_2 vertical columns during summertime in the eastern United States. In this new product, OMI NO_2 tropospheric columns increase by up to 160 % in city centers, and decrease by 20 – 50 % in the rural areas outside of urban areas when compared to the operational NASA product. Our new product shows much better agreement with the Pandora NO_2 and Airborne Compact Atmospheric Mapper (ACAM) NO_2 spectrometer measurements acquired during the DISCOVER-AQ Maryland field campaign. Furthermore, the correlation between our satellite product and EPA NO_2 monitors in urban areas has improved dramatically: r^2 = 0.60 in new product, r^2 = 0.39 in operational product, signifying that this new product is a better indicator of surface concentrations than the operational product. Our work emphasizes the need to use both high-resolution and high-fidelity models in order to re-calculate satellite data in areas with large spatial heterogeneities in NO_x emissions. Although the current work is focused on the eastern United States, the methodology developed in this work can be applied to other world regions to produce high-quality region-specific NO_2 satellite retrievals.

1 Introduction

Tropospheric NO_2 is a trace gas toxic to human health and during ideal atmospheric conditions can photolyze to create O_3 another toxic air pollutant with a longer atmospheric lifetime. The eventual fate of tropospheric NO_2 is often HNO_3, a chemical species easily dissolved in water and responsible for acid rain. HNO_3 can also react with ammonia to create nitrate aerosols, which contribute to haze and are harmful to human health.

There are some natural sources of nitrogen oxides ($NO_x \equiv NO+NO_2$), such as from soil through microbial nitrification and denitrification (Conrad, 1996), lightning (Ridley et al., 1996), and natural wildfires (Val Martin et al., 2006), but the majority of the NO_2 in our atmosphere today originates from anthropogenic sources (van Vuuren et al., 2011). When temperatures are greater than 1500 K, such as in fuel combustion, nitrogen (N_2) and oxygen (O_2) spontaneously react to create NO via the endothermic Zeldovich mechanism. The nitrogen in fuels are also converted to NO during combustion making fuels rich in nitrogen, such as coal, more efficient in creating NO. NO is quickly oxidized to NO_2 in the atmosphere, most often by ozone, in a matter of seconds. Thus the NO and NO_2 species are often grouped into a single species called NO_x. In the presence of hydroperoxy (HO_2) or organic peroxy radicals (RO_2, where R is any organic group), NO can also be oxidized to NO_2 without consuming ozone. This is the rate-limiting step in the chemical chain reaction producing tropospheric ozone.

NO_2 has strong absorption features within the 400 – 450 nm wavelength region (Vandaele et al., 1998), which approximately corresponds to violet visible light. Satellite instruments measure the absorption of solar backscatter in the UV-visible spectral range, enabling estimation of the amount of NO_2 in the atmosphere between the instrument and the surface. By comparing observed spectra with a reference spectrum, we can derive total column amounts; this technique is called differential optical absorption spectroscopy (DOAS) (Platt, 1994).

NO_2 has been continuously measured from satellites for over two decades now. The first instrument to remotely measure NO_2 was the Global Ozone Monitoring Experiment (GOME) launched aboard the European Remote Sensing 2 (ERS-2) satellite in April 1995 (Burrows et al., 1999). Despite its coarse temporal and spatial resolution (global coverage once every three days and pixel size of 40 × 320 km), it was the first remotely sensed instrument to characterize NO_2 columns from space, showing enhanced tropospheric NO_2 over North America and Europe (Martin et al., 2002; Martin et al., 2003). In the early 2000s, Scanning Imaging Absorption Spectrometer for Atmospheric Chartography (SCIAMACHY) (Bovensmann et al., 1999) and Ozone Monitoring Instrument (OMI) (Levelt et al., 2006; Bucsela at el., 2006; Boersma et al., 2007) became additional space-based instruments to measure NO_2. These instruments were designed to achieve better spatial resolution (SCIAMACHY: 30 × 60 km, OMI: 13 × 24 km) than GOME. Boersma et al. (2008a) documented the differences between the two retrievals. In early 2012, ground operators lost contact with SCIAMACHY, but OMI is still operational as of 2017. There are two operational OMI NO_2 retrievals: the KNMI DOMINO v2.0 product (Boersma et al., 2007) and the NASA OMNO2 v3.0 product (Krotkov et al., 2017).

OMI NO_2 has been used to estimate NO_x emissions from various areas around the globe (Streets et al., 2013) including North America (Boersma et al., 2008b; Lu et al., 2015), Asia (Zhang et al., 2008; Han et al, 2015; Kuhlmann et al., 2015), the Middle East (Beirle et al., 2011), and Europe (Huijnen et al., 2010; Curier et al., 2014). It has also been used to generate and validate NO_x emission estimates from source sectors such as soil (Hudman et al., 2010; Vinken et al., 2014a; Rasool et al., 2016), lightning (Allen et al., 2012; Liaskos et al., 2015; Pickering et al., 2016), power plants (de Foy et al., 2015), aircraft (Pujadas et al., 2011), marine vessels (Vinken et al., 2014b; Boersma et al., 2015), and urban centers (Lu et al., 2015; Canty et al., 2015; Souri et al., 2016). More recently, there has been an emphasis on analyzing emission trends because OMI has been retrieving high-quality tropospheric NO_2 data for over ten years. Over this decade, some areas have seen increases, such as India (Lu and Streets, 2012), the Canadian oil sands region (McLinden et al., 2015), and other oil extraction regions (Duncan et al., 2016), while areas such as the eastern United States (Russell et al., 2012; Lamsal et al., 2015; Krotkov et al., 2016; de Foy et al., 2016a) and Europe (Curier et al., 2014; Duncan et al., 2016) have seen large decreases due to a switch to cleaner fuels and the implementation of emission control technologies. Over this 10-year period, China has seen a reversal of its trends: during 2005-2010 OMI NO_2 tropospheric columns were increasing (Verstraeten et al., 2015), in 2011-2012 they had stabilized (Souri et al., 2017), and since 2012 they have subsequently decreased as the country enforces its Twelfth 5-year plan (de Foy et al., 2016b).

Remote sensing instruments typically measure the entire column content instead of in situ concentrations at individual vertical levels. Being able to derive surface concentrations from column content information would be very useful for the policy-making and health-assessment communities. In particular, detecting the spatial heterogeneities of NO_2 in and around city centers are of strong interest as many people are exposed to NO_2 or co-located pollutants exceeding policy thresholds in these areas. Satellite measurements with spatial resolution > 13 km, such as OMI, have difficulty observing the fine structure of NO_2 plumes at or near the surface (e.g., highways, power plants, factories, etc.) (Chen et al., 2009; Ma et al., 2013; Flynn et al., 2014), which are often less than 10 km in width (Heue et al., 2008). This can lead to a spatial smoothing of pollution, which does not exist in reality (Hilboll et al., 2013). Remote sensing instruments with finer spatial resolution, such as TROPOMI (Veefkind et al., 2012) and TEMPO (Zoogman et al., 2017), may be able to resolve this issue.

Until the next generation of satellites is launched, there have been several techniques to modify OMI NO_2 data a posteriori. Kim et al. (2016) developed a technique in which users can utilize regional air quality model information to spatially downscale OMI NO_2 measurements. This technique has shown to increase the variability of OMI NO_2 within urban areas, which is in better agreement with observations in these regions. In another effort to merge model and satellite data, Lamsal et al. (2008) was able to infer surface level NO_2 concentrations from OMI NO_2 by applying local scaling factors from a global model. There has also been an emergence of a technique that combines land-use regression techniques with satellite information to infer ground-level NO_2 concentrations (Novotny et al., 2011; Vienneau et al., 2013; Lee et al., 2014; Bechle et al., 2015; Young et al., 2016). While each individual technique is useful, all of the aforementioned techniques use model data to adjust existing satellite data, but do not address issues inherent with the satellite retrieval methodology.

Previous studies have shown that the air mass factor, a value needed to convert the slant column measurement into a vertical column amount, is one of the largest source of uncertainty in the OMI NO_2 retrieval, contributing up to half of the total error (Boersma et al., 2004; Lorente et al., 2017). There are two existing OMI NO_2 products that use information from a regional chemical transport model to re-calculate the air mass factor: Berkeley High-Resolution (BeHR) NO_2 (Russell et al., 2011; Laughner et al., 2016) and City University of Hong Kong OMI (HKOMI) NO_2 (Kuhlmann et al., 2015). BeHR NO_2 uses a monthly averaged 12 × 12 km Weather Research and Forecasting coupled with Chemistry (WRF-Chem) model simulation with higher resolution terrain pressure and Moderate-resolution Imaging Spectroradiometer (MODIS) black-sky albedo to re-calculate the air-mass factors for the United States. This study found that by updating the air mass factors with a high-resolution simulation, NO_2 tropospheric vertical columns increased in urban areas and decreased in rural areas when compared to typical satellite products processed with global model simulations (Russell et al., 2011). More recently, the BeHR NO_2 product has been updated (summer 2013 only) to account for daily variations in shape profiles and terrain pressure, which modifies daily retrievals by as much as 40% (Laughner et al., 2016). The HKOMI product uses NO_2 shape profile, terrain elevation, and meteorological information from a 3 × 3 km a Community Multiscale Air Quality (CMAQ) simulation coupled offline to a Weather Research and Forecasting (WRF) simulation to re-calculate the air mass factor for the Pearl River Delta region of China. Similarly, they found that the tropospheric vertical NO_2 columns increased in an urban area; this improved agreement between satellite and ground observations (Kuhlmann et al., 2015). One critical limitation of the BeHR and HKOMI products is the lack of lightning NO_x emissions in the model simulations used to derive the air mass factor. The POMINO product takes a slightly different approach. This study improves the air mass factor for China (Lin et al., 2015) by (1) using improved information on surface albedo (MODIS Bidirectional Reflectance Distribution Function (BRDF)), (2) improving the treatment of aerosols and cloud pressure/fraction, and (3) using a nested (0.667° × 0.5°) GEOS-Chem simulation for the NO_2 shape profiles. These three changes increase annual mean NO_2 tropospheric vertical columns by 15 – 40%. A summary of all available OMI NO_2 retrievals are listed in Table 1.

We build upon these studies by using an even higher resolution (1.33 km) regional air quality model to generate air mass factors for urban metropolitan areas in the mid-Atlantic region of the eastern United States. Use of such resolution allows calculation of air mass factors representing OMI ground pixels. The new air mass factors are then used to re-calculate NO_2 tropospheric vertical columns. Furthermore we utilize a technique for constraining the NO_2 shape profiles to aircraft observations and invoke a new downscaling method developed by Kim et al., (2016) to enhance the content of the satellite observations.

2 Methods

2.1 OMI NO_2

The Ozone Monitoring Instrument (OMI) has been operational on NASA's Earth Observing System (EOS) Aura satellite since October 2004 (Levelt et al., 2006). The satellite follows a sun-synchronous, low-earth (705 km) orbit with an equator overpass time of approximately 13:45 local time. OMI measures total column amounts in a 2600

km swath divided into 60 unequal area "field-of-views", or pixels. At nadir (center of the swath), pixel size is 13 × 24 km, but at the swath edges, pixels can be as large as 26 × 128 km. In a single orbit, OMI measures approximately 1650 swaths and achieves daily global coverage over 14 – 15 orbits (99 minutes per orbit). OMI measures solar backscatter within the 270-500 nm wavelength range. For this paper, we focus on the NO_2 retrieval which is derived from measurements in the 400 – 450 nm range. Since June 2007, there has been a partial blockage of the detector's full field of view, which has limited the number of valid measurements; this is known in the community as the row anomaly: http://projects.knmi.nl/omi/research/product/rowanomaly-background.php.

OMI measures radiance data between the instrument's detector and the Earth's surface. Comparison of these measurements with a reference spectrum (i.e., DOAS technique), allows for calculation of the total slant column density (SCD), which represents the integrated NO_2 abundance from the sun to the surface, through the atmosphere, to the instrument's detector. For tropospheric air quality studies, vertical column density (VCD) NO_2 data are more appropriate. This is done by subtracting the stratospheric slant column from the total (tropospheric + stratospheric) slant column and dividing by the tropospheric air mass factor (AMF), which is defined as the ratio of the SCD to the VCD, as shown in Eq. (1):

$$VCD_{trop} = \frac{SCD_{total} - SCD_{strat}}{AMF_{trop}} \quad \text{, where } AMF_{trop} = \frac{SCD_{trop}}{VCD_{trop}} \tag{1}$$

The tropospheric AMF has been derived to be a function of the optical atmospheric/surface properties (surface albedo, aerosols, cloud fraction, and cloud height) and a priori NO_2 shape profile (Palmer et al., 2001; Martin et al., 2002) and can be calculated as follows (Lamsal et al., 2014) in Eq. (2):

$$AMF_{trop} = \frac{\sum_{surface}^{tropopause} SW \times x_a}{\sum_{surface}^{tropopause} x_a} \tag{2}$$

Where x_a is the partial column NO_2. The optical atmospheric/surface properties are characterized by the scattering weight (SW) and are calculated by a forward radiative transfer model (TOMRAD), which are output as a look-up table (LUT). The SWs are then adjusted real-time depending on observed viewing angles, surface albedo, cloud fraction, and cloud pressure. For this study, we follow previous studies (e.g., Palmer et al., 2001, Martin et al., 2002, Boersma et al., 2011, Bucsela et al., 2013) and assume that SWs and NO_2 profile shapes are independent. The a priori NO_2 profile shapes (x_a) must be provided by a model simulation. In an operational setting, NASA uses a monthly-averaged and year-specific Global Model Initiative (GMI) model (1.25° lon × 1° lat; ~110 km × 110 km in the mid-latitudes) simulation to provide the a priori NO_2 shape profiles. For this study, we derive tropospheric VCDs using a priori NO_2 shape profiles from a regional CMAQ simulation. A description of this methodology is included in Section 2.5. All other parameters from the NASA Level 2 product including the total SCD, the stratospheric SCD (which is inferred using a local analysis of the stratospheric field (Bucsela et al., 2013)), the OMI O_2-O_2 cloud pressure/fraction algorithm (which uses a look-up table to convert O_2-O_2 column density and continuum reflectance into cloud pressure/fraction (Acarreta et al., 2004)), the surface albedo (which is derived from OMI Lambert Equivalent Reflectance (LER) (Kleipool et al., 2008)), and the SW remain unchanged.

We filter the Level 2 OMI NO_2 data to ensure only valid pixels are used. Daily pixels with solar zenith angles ≥ 80°, cloud radiance fractions ≥ 0.5, or surface albedo ≥ 0.3 are removed as well as the five largest pixels at the swath edges (i.e., pixel numbers 1 – 5 and 56 – 60). Finally, we remove any pixel flagged by NASA including pixels with NaN values, 'XTrackQualityFlags' ≠ 0 or 255 (RA flag), or 'VcdQualityFlags' > 0 and least significant bit ≠ 0 (ground pixel flag).

2.2 DISCOVER-AQ NO_2 observations

In the validation of our new satellite product, we use in situ NO_2 observations from the DISCOVER-AQ Maryland field campaign. DISCOVER-AQ was a four-part field experiment designed to probe the atmosphere near urban areas in excruciating detail from aircrafts, ground station networks, and satellites. The first experimental campaign took place in Maryland (Baltimore, MD - Washington D.C. area) in July 2011. This campaign was particularly unique for an aircraft field campaign in that the focus was limited to single metropolitan area, whereas in other aircraft campaigns, spatial coverage is often over a larger domain. We utilize data acquired by four sources during this campaign: the P3-B aircraft, the ground-based Pandora spectrometer network, the Airborne Compact Atmospheric Mapper on the UC-12 aircraft, and the long-term EPA ground monitoring network. A typical P3-B aircraft and UC-12 flight path, Pandora NO_2 spectrometer locations, and ground monitor locations are shown in Figure 1. DISCOVER-AQ observations were retrieved from the online data archive: http://www-air.larc.nasa.gov/cgi-bin/ArcView/discover-aq.dc-2011. A further description of DISCOVER-AQ Maryland can be found in Crawford et al. (2014).

2.2.1 P3-B aircraft data

We use P3-B aircraft NO_2 data gathered by the Cohen group (instrument reference: (Day et al, 2002)) to assess the accuracy of our model simulation. This instrument does not have the same positive bias as chemiluminescence NO_2 detectors, so there is no need to modify NO_2 concentrations by applying an empirical equation (e.g., Lamsal et al., 2008). We utilize one-minute averaged P3-B data from all fourteen flights during July 2011. One-minute averaged data is already pre-generated in the data archive. Hourly output from our model simulation is spatially and temporally matched to the observations. We then bin the data into different altitude ranges for our comparison.

2.2.2 Pandora NO_2 data

Measurements of total column NO_2 from the Pandora spectrometer (instrument reference: (Herman et al., 2009)) are used to evaluate the OMI NO_2 satellite products. Valid OMI NO_2 pixels are matched spatially and temporally to Pandora total column NO_2 observations. To smooth the data and eliminate brief small-scale plumes or anomalies, we average the Pandora observations over a two hour period (± one hour of the overpass time) before matching to the OMI NO_2 data. During July 2011, there were twelve Pandora NO_2 spectrometers operating during the experiment; this corresponded to only seventy-nine instances in which valid Pandora NO_2 observations matched valid OMI NO_2 column data.

2.2.3 Airborne Compact Atmospheric Mapper (ACAM) NO_2 data

The UC-12 aircraft was outfitted with a downward looking spectrometer called the Airbone Compact Atmospheric Mapper (ACAM) during the DISCOVER-AQ Maryland campaign (instrument reference: (Kowalewski and Janz, 2009)). The instrument collects hyperspectral measurements in the UV, visible, and near-infrared range from an altitude of approximately 8 km. From these measurements, tropospheric column NO_2 underneath the aircraft can be calculated (Lamsal et al., 2017). An ACAM pixel is considered valid, if there are no clouds between the instrument's detector and the surface. Valid OMI NO_2 pixels are matched spatially and temporally (± one hour of the satellite overpass time) to the ACAM column NO_2 observations. During July 2011, there were only six days in which the UC-12 flight paths overlapped an OMI NO_2 swath; this corresponded to only 107 OMI NO_2 pixels which could be compared to the ACAM NO_2.

2.2.4 EPA ground monitor data

There are eighteen EPA NO_2 monitoring sites within our study area that were operational during the 5-year period of interest. We gathered this data from the EPA AQS Data Mart (EPA, 2016). Monitoring data were filtered so that only days with valid satellite data were included. To smooth the data, we average all valid ground observations between 12 – 4 PM local time. All EPA monitors measure NO_2 by the chemiluminescence method which has a high bias when compared to other techniques (Dunlea et al., 2007; Lamsal et al., 2008; Lamsal et al., 2015). Dunlea et al. (2007) has shown the high bias to be 22 % in a polluted urban environment and as large as 50 % during the mid-afternoon. Lamsal et al. (2008) suggests the bias may be even higher, 50 – 65 %, in the eastern U.S. during the summertime. For this reason, we refer to NO_2 from these monitors as NO_2*.

2.3 GMI model simulation

The operational NASA OMI NO_2 product uses a Global Modeling Initiative (GMI) (Strahan et al., 2007) model simulation with a horizontal resolution of 1° × 1.25° (~110 × 110 km) sampled at the OMI overpass time to calculate a priori NO_2 shape factors. The model is driven by assimilated meteorological fields from the Goddard Earth Observing System (GEOS) at the NASA Global Modeling and Assimilation Office (GMAO, ttp://gmao.gsfc.nasa.gov/). The GEOS-5 meteorological data are provided every 3–6 h (3 h for surface fields and mixing depths) at 72 pressure levels in the vertical, extending from surface to 0.01 hPa. The model includes the latest available inventories for anthropogenic emissions as discussed in Strode et al. (2015) and Krotkov et al. (2017). These emissions are updated annually with annual scale factor estimates provided by individual countries (van Donkelaar et al., 2008). The GMI model also includes NO_x emissions from soil, lightning, biomass burning, biofuel, and aircraft sources, as described in Duncan et al. (2007) with updates as discussed in Krotkov et al. (2017). The GMI simulation is conducted for 2004-2014, sampling hourly model output at the OMI overpass time. The standard operational retrieval is based on yearly-varying monthly average NO_2 profiles derived from the GMI simulation.

2.4 CMAQ model simulation

For the high-resolution OMI NO_2 product, we use a CMAQ regional model simulation initially prepared for use in Loughner et al. (2014). CMAQ v5.0 is driven off-line by meteorological inputs from the WRF model v3.3 for June and July 2011. Horizontal spatial resolution of both WRF and CMAQ is at 1.33 km. Both models also include 34 vertical levels between the surface and 100 hPa, with 16 layers within the lowest 2 km. The ACM2 drives the boundary layer parametrization in WRF, while ACM computes the convective mixing in CMAQ. Anthropogenic emissions are projected to 2012 from the 2005 EPA National Emissions Inventory (NEI); the 2011 NEI was unavailable when this model simulation was originally completed. Biogenic and lightning emissions are calculated online; biogenic emissions are calculated using BEIS v3.14. Soil NO_x emissions are not included here because the CMAQ soil NO_x parametrization was implemented in a newer version of the model (Rasool et al., 2016). This model simulation utilizes CB05 gas-phase chemistry. The 1.33 km simulation, which we use exclusively in this study, is nested inside three larger domains: 36 km, 12 km, and 4 km. Boundary conditions for the 36 km domain are provided by the MOZART-4 global model. The top of the model assumes "zero gradient", which means the top boundary has concentrations equal to the top model layer. The CMAQ 1.33 km model domain is shown in Figure 1. For additional details, including a discussion on the uncertainty of the meteorological and chemical fields in this simulation, please reference Loughner et al. (2014). Our study is particularly unique in that we use a 1.33 km simulation in lieu of a model with a horizontal resolution more typical of OMI (>13 km). We do this so that we can capture the fine-scale variability within urban areas that cannot be simulated by coarser models and observations.

2.5 Air Mass Factor Re-Calculation using CMAQ

To re-calculate the air mass factor for each OMI pixel, we first compute interim air mass factors for each CMAQ model grid cell. The interim air mass factor for each CMAQ grid cell is a function of the NO_2 shape factor from the model grid cell and scattering weight from the OMI pixel that overlaps it. We then average all interim air mass factors within an OMI pixel (usually 100's) to generate a single tropospheric air mass factor for each individual OMI pixel. This new air mass factor is used to convert the total slant column into a tropospheric vertical column using Equation 1. Model outputs were sampled at the local time of OMI overpass. For June and July 2011, we use daily NO_2 profiles and terrain pressures (e.g., (Laughner et al., 2016)) to re-calculate the AMF. For years other than 2011, we used 2011 monthly mean values of NO_2, temperature, and tropopause pressures for the calculation of the AMF. Once the tropospheric vertical column of each OMI pixel was re-calculated, the product was oversampled for June and July over a 5-year period (2008-2012; 10 months total).

3 Results

In this section, we describe the new high-resolution satellite product and our validation efforts. Unless otherwise noted, all OMI NO_2 results presented here are vertical column densities. First, we compare a priori NO_2 shape profiles simulated by GMI (global model) and CMAQ (regional model). Next we develop an initial OMI NO_2 satellite product (OMI_CMAQ) using AMFs generated from the CMAQ a priori NO_2 profiles. We introduce two

additional steps: improving a priori NO_2 shape profiles using aircraft observations and applying a spatial weighting kernel to further improve the spatial distribution of NO_2. We then evaluate our new product by comparing to DISCOVER-AQ observations. And finally, we compare the new OMI NO_2 product with NO_2 VCDs from the original CMAQ simulation.

3.1 Evaluating modeled NO_2 shape profiles: GMI vs. CMAQ

Trace gas shape profiles provided by model simulations are a critical input to satellite retrievals. To understand the effects of model choice on the a priori NO_2 shape profile, we compare the mean 2 PM local time tropospheric NO_2 vertical profiles from CMAQ and GMI at several locations in the mid-Atlantic during June & July 2011. In the left panels of Figure 2, we show the mean NO_2 mixing ratio as function of altitude for three locations: downtown Baltimore Maryland (an urban area), the Morgantown Power Plant located in Newburg, Maryland 60 km south of the District of Columbia (D.C.), and Arendtsville, Pennsylvania (rural), a location 100 km northwest of Baltimore and upwind of major metropolitan areas during days with climatologically westerly winds. All three locations are shown on Figure 1. In Baltimore, GMI simulates a mean 2 PM surface NO_2 mixing ratio of 2.2 ppbv, while CMAQ simulates 9.6 ppbv at the same location. The "Oldtown" monitoring site in Baltimore registered a surface NO_2* mixing ratio of 10.5 ppbv within +/- 2 hours of valid co-located satellite overpasses. As discussed in Sect. 2.2.4, the corrected surface NO_2 mixing ratio is approximately 22% lower (but may be up to 65% lower) than observed NO_2*; our best surface estimate of 8.2 ppbv with error bars [3.7, 10.5] is shown by the black triangle on Figure 2. The surface value simulated by CMAQ (9.6 ppbv) is much closer to the observed value than GMI (2.2 ppbv). In the second row of panels, the panels representing the Morgantown power plant, CMAQ simulates a plume of NO_2 above the surface; the max value is 11.8 ppb corresponding to an altitude of 460 m. The GMI simulation cannot resolve power plant plumes. This yields significant errors in the NO_2 shape profiles simulated by GMI near observed large point sources. In the bottom row of panels, we show a location in rural Pennsylvania. CMAQ, once again, does better in simulating the surface concentration than GMI.

However, in the free troposphere (i.e., above 3 km and below the tropopause) CMAQ consistently simulates smaller NO_2 than GMI. CMAQ simulates NO_2 mixing ratios between 0.01- 0.04 ppbv, while GMI simulates NO_2 mixing ratios between 0.06 – 0.09 ppbv over the same altitudes; GMI simulates values which are a factor of three higher than CMAQ. To determine whether lightning NO is the primary driver of this difference, we compare lightning NO emissions from both model simulations in Figure 3. The CMAQ model ingests lightning NO emissions that are an order of magnitude larger than the GMI simulation at most altitudes. This is likely due to WRF simulating more convective precipitation and higher cloud-top heights, both input variables to the lightning NO parameterization, than GMI. Therefore, the differences in free tropospheric NO_2 between the two models do not arise from the lightning NO_x parameterizations, but instead from a combination of the chemistry, aviation emissions, vertical mixing, long-range transport, and stratospheric-tropospheric exchange.

3.2 Calculation of air mass factors: GMI vs. CMAQ

A normalization of the NO_2 as a function of altitude (i.e., $x_a / \Sigma x_a$ in Eq. (2)) is the next step in the calculation of the AMF; these values are defined in the literature as shape factors. The center column panels show NO_2 shape factors for three locations. In Figure 2b (Baltimore), the GMI and CMAQ shape profiles (i.e., shape factors as a function of altitude) appear to be similar, but there are noticeable differences within the boundary layer and free troposphere. In Figure 2e, CMAQ captures a localized power plant plume, while GMI does not; this yields large differences in the shape profile within the boundary layer. And in Figure 2h, CMAQ suggests that the NO_2 gradient near the surface is not as sharp.

Since the AMF is also a function of the SW, small differences in NO_2 shape profiles can manifest very different AMFs. For example, small differences in the shape profile at 7.5 km, where the SW is a maximum (SW = 2.9), have an order of magnitude larger effect than differences at the surface (SW = 0.4).

To fully understand the differences caused by the new NO_2 shape factors, we multiply the two shape factors by the satellite scattering weights. Here we define the shape factors × scattering weight ((i.e., $(x_a \times SW)/ \Sigma x_a$ in Eq. (2)) as the adjusted shape factors. This is analogous to the values used for calculation of the air mass factor. The AMF is the integral of the adjusted shape factors with respect to height. In Figure 2c, the CMAQ adjusted shape profile shows values much closer to zero above 3 km than GMI. By using a priori shape profiles from CMAQ, we are enhancing the sensitivity of satellite observations to NO_2 concentrations within the boundary layer in Baltimore. In Figure 2f, the adjusted shape profiles are even more dramatic. At this location, adjusted shape profile values from CMAQ are relatively large below 1 km, and close to zero above 1 km, while GMI shows nearly an order of magnitude larger sensitivity above 1 km. In Figure 2i, CMAQ shows larger values above the surface, but within the boundary layer, while GMI shows larger values directly at the surface. In areas, such as these, the adjusted shape factors yield only small changes. In Figures 2c and 2f, the area underneath the red curve is smaller than the area underneath the blue curve. This will yield smaller AMFs when using CMAQ at these locations. As a result, we should expect the new OMI tropospheric NO_2 columns to be larger near urban areas and point sources which cannot be resolved by global models. At the rural location, the areas underneath the two curves are roughly the same, yielding similar AMFs and NO_2 columns.

3.3 Calculation of OMI tropospheric column NO_2

3.3.1 Using CMAQ profiles

We use the AMFs based off the CMAQ simulation to generate NO_2 tropospheric column amounts; we call this the OMI_CMAQ product. For this product, tropospheric NO_2 columns are calculated from the NASA Level 2 OMI NO_2 total slant column using Eq. (1). For AMFs calculated in the months of June and July 2011, we use AMFs derived from daily NO_2 shape factors as described by Laughner et al. (2016), resulting in more day-to-day variability in the AMF. Daily CMAQ NO_2 shape profiles from the hourly output are matched temporally and

spatially to the OMI pixel. For years other than 2011, we use a two-month (June and July) average of the 2011 NO_2 shape factors to derive "summertime" AMFs. Since the resolution of CMAQ is finer than the resolution of OMI, we average all CMAQ AMFs across each individual pixel. Often there are over two-hundred CMAQ AMFs within a single pixel. Since CMAQ is capturing the spatial heterogeneities in urban areas, using it in lieu of GMI to provide NO_2 shape profiles can yield large variability in the AMF between adjacent OMI pixels.

Figures 4a and 4b depict the OMI NO_2 tropospheric columns using a priori shape profile information from GMI (OMI_GMI; Figure 4a) and CMAQ (OMI_CMAQ; Figure 4b) in calculating the AMF. Both products are oversampled to 1.33 km for June & July over a 5-year period (2008-2012) by re-gridding to the CMAQ model grid and then averaging the data over the 10-month (two months × five years) period. We have chosen the June & July timeframe because the CMAQ simulation is only available during these two months. For the OMI_GMI product, the tropospheric NO_2 columns were taken directly from the NASA OMI NO_2 v3.0 Level 2 product. Figure 5a shows the ratio between the two products.

In the new product (OMI_CMAQ), there are large increases of the NO_2 VCDs in city centers. In the operational OMI_GMI product, over the 5-year period, the maximum tropospheric NO_2 column within Baltimore city limits is 3.9×10^{15} molecules per cm^2. By contrast, in the OMI_CMAQ product, the maximum tropospheric NO_2 column within Baltimore city limits is 7.2×10^{15} molecules per cm^2. These results indicate that by using a regional model, the tropospheric NO_2 VCDs in urban areas rise dramatically. This is due, in part, to the regional model being able to better capture NO_2 concentrations in the lower-most part of the troposphere (i.e., Figure 2). In suburban and rural locations, NO_2 tropospheric VCDs are roughly the same. For example, at the rural Pennsylvania (Arendtsville) location, the NO_2 tropospheric column in the operational product is 2.8×10^{15} molecules per cm^2 and 2.7×10^{15} molecules per cm^2 in the new OMI_CMAQ product.

3.3.2 Improving modeled vertical profile information with in situ observations

While using CMAQ to calculate AMFs yields a marked improvement in simulating profile shape when compared to using GMI, this CMAQ simulation has a high bias in the calculation of total reactive nitrogen oxides (NO_y) (Goldberg et al., 2014; Anderson et al., 2014), which must be accounted for. Many literature sources, including others using different model set-ups (all are based on the NEI), also show a high bias in simulating summertime column NO_2 (Canty et al., 2015; Souri et al., 2016), NO_x (Travis et al., 2016), and NO_y (Goldberg et al., 2016).

In Figure 6, we show NO_2 observations acquired by the P3-B aircraft in the early afternoon between 300 m and 3 km during DISCOVER-AQ Maryland matched to CMAQ and GMI output. NO_2 mixing ratios simulated by CMAQ are consistently larger throughout the mid- and upper-boundary layer and lower free troposphere (1 – 3 km) by up to a factor of three, but there is fairly good agreement below 1 km; similar results were found by Flynn et al. (2016). The NO_2 mixing ratios simulated by GMI below 1 km are a factor of two lower than the P3-B observations. Furthermore, the variability is an order of magnitude smaller than the observations. These shortcomings of GMI are a result of using a monthly mean (the same value used for the satellite retrieval) and coarse resolution model.

Since the P3-B aircraft has limited measurements above 3 km, we have to use estimates from other literature sources to determine the validity of CMAQ in the free troposphere. Lamsal et al. (2017) used measurements from the Airborne Compact Atmospheric Mapper (ACAM) to deduce that GMI is better than CMAQ at simulating NO_2 in the free troposphere. In the upper free troposphere, above 10.5 km, Travis et al. (2016) note that NO_2 is significantly underestimated by global models, such as GMI. As shown in Figure 2, CMAQ simulates even lower NO_2 concentrations than GMI at these altitudes.

We apply a scaling factor inferred from in situ aircraft observations to account for the high model bias below 3 km, and low model bias above 3 km; this is a simplified form of data assimilation. Below 3 km, the model was scaled to observations from the P3-B by multiplying the original values at these altitudes by the fraction of NO_2 actually observed. For example, modeled NO_2 between 1000 – 1500 m was multiplied by 0.63 to account for the model high bias within this altitude bin. This procedure was repeated for all altitude bins in 500-m intervals from the surface up to 3 km. It should be noted that aircraft measurements from the DISCOVER-AQ Maryland campaign took place only within the Baltimore metropolitan region, and thus these scaling factors may not be fully applicable to upwind rural regions, and certainly cannot be applied to locations outside the eastern United States. Between the altitudes of 3 km – 10.5 km, we switched out the NO_2 mixing ratios from CMAQ for NO_2 mixing ratios from GMI. Between 10.5 km and the tropopause, we use GMI NO_2 mixing ratios multiplied by a factor of three; this scaling factor is based on summertime NO_2 observations during the SEAC^{4}RS field campaign as described by Travis et al. (2016).

Using these scaled mixing ratios, we then re-calculate the AMFs and corresponding tropospheric NO_2 columns. Figure 4c shows observationally-constrained OMI_CMAQ (OMI_CMAQ_O) tropospheric NO_2 columns during the same 5-year summertime period. NO_2 tropospheric columns in this product are smaller in magnitude than OMI_CMAQ, and yet still noticeably larger in urban areas than the operational OMI_GMI retrieval (i.e., in Baltimore OMI_GMI: 3.9×10^{15} , OMI_CMAQ: 7.2×10^{15}, OMI_CMAQ_O: 5.0×10^{15}). Retrievals in upwind rural areas in this new product are now lower than the operational product (i.e., in Arendtsville OMI_GMI: 2.8×10^{15} , OMI_CMAQ: 2.7×10^{15}, OMI_CMAQ_O: 1.7×10^{15}).

The large reduction in NO_2 tropospheric columns between OMI_CMAQ and OMI_CMAQ_O is an outcome of using larger AMFs. The larger AMFs are a result of the original overestimate within the boundary layer and underestimate in the free troposphere. This is a particularly important finding because it means that a model with large biases in the simulation of NO_2 can yield poor tropospheric vertical column contents, despite high spatial resolution. This emphasizes the need to evaluate the emissions and chemistry of a model before it is used for satellite retrievals.

3.3.3 Enhancing spatial resolution with spatial weighting kernels

Finally in a last step, we apply the method described by Kim et al. (2016) to downscale the OMI retrieval. This method applies a spatial-weighting kernel to portions of each pixel based on the estimated influence from each locality within the pixel. For example, if one side of a pixel overlaps a polluted region, while the other side of the

pixel overlaps a cleaner area, the operational OMI product will denote that the entire area is moderately polluted. Instead, we weight portions of the individual pixel based on the variability simulated in CMAQ. Using this method, the quantity of the satellite data is numerically preserved. This yields a higher resolution snapshot of tropospheric column NO_2 that is still constrained by satellite data. Please reference Kim et al. (2016) for a visual representation of this method.

We call this product OMI_CMAQ observationally-constrained + downscaled (OMI_CMAQ_OD). Figure 4d shows OMI_CMAQ_OD tropospheric NO_2 columns. There is now large variability throughout the region, which is typical of a pollutant with a short lifetime (< 1 day) such as NO_2 in the summertime. NO_2 tropospheric columns in urban cores are now significantly larger than the operational product, (i.e., in Baltimore OMI_GMI: 3.9×10^{15}, OMI_CMAQ_OD: 10.2×10^{15}). The largest increases occur near power plants, cement kilns, and major highways. OMI_CMAQ_OD in upwind rural areas are 20 – 50 % lower than the operational product (i.e., in Arendtsville OMI_GMI: 2.8×10^{15}, OMI_CMAQ_OD: 1.6×10^{15}).

While this new product shows power plant plumes that are two to three times larger, we are not suggesting that emissions from power plants are larger than we thought. Instead we are suggesting that the spatially downscaled OMI product can now "see" these individual plumes, whereas in the operational product, these plumes are blended into an average across the entire OMI pixel. In rare cases, oversampling the operational product in and around very large rural point sources, can denote large power plant plumes (deFoy et al., 2015), but up until this point, smaller point sources or localized sources near major urban areas could not be seen in an OMI NO_2 product.

3.4 Comparison of satellite products to in situ observations

3.4.1 Comparison to the Pandora NO_2 spectrometer network

During DISCOVER-AQ Maryland, total column NO_2 was measured by a network of twelve Pandora instruments (Herman et al., 2009). We match daily valid Pandora NO_2 and valid satellite overpass information, and plot the information in Figure 7a. To calculate total OMI columns, we add the vertical stratospheric column information, a variable in the NASA OMI NO_2 Level 2 files, to the OMI tropospheric retrievals. While the operational product (OMI_GMI) shows some agreement at low values, it has poor agreement when observed NO_2 column amounts are greater than 10×10^{15} cm^{-2}. This is due to coarse resolution of OMI pixels (24 × 13 km at nadir) and the AMFs computed with GMI a priori NO_2 profiles, among potential other factors. The slope of the OMI_GMI best-fit line is 0.44, representing a striking low bias at high values, and the $r^2 = 0.10$ denoting almost no correlation; similar results were found by Ialongo et al. (2016).

Table 2 shows the statistical comparison between the satellite products and observations. All OMI_CMAQ products yield slopes closer to one indicating that they are better at capturing the variability between low and high values observed by the ground monitors. The OMI_CMAQ_OD product eliminates the bias altogether. The slope of the OMI_CMAQ_OD best-fit is 0.99 and the r^2 increases. An improved but still low r^2-value in the newest product may

indicate that a 1.33 km CMAQ simulation provides an improvement, but not an identical match, of daily NO_x emissions and fine-scale winds responsible for plume dispersion. Furthermore, we cannot expect the satellite to match the exact spatial heterogeneity observed by the point measurements from Pandora because these instruments observe a very narrow fraction of the atmosphere and measure column NO_2 in a fundamentally different manner.

3.4.2 Comparison to the Airborne Compact Atmospheric Mapper (ACAM) spectrometer NO_2

The ACAM NO_2 instrument acquired measurements of tropospheric column NO_2 below altitudes of 8 km during DISCOVER-AQ Maryland. We match ACAM NO_2 measurements within ± one hour of the OMI overpass time to valid OMI NO_2 measurements. The comparison is plotted in Figure 8. Both the slope and r^2-value of the new OMI_CMAQ_OD product are closer to one when compared to the OMI_GMI product indicating that the OMI_CMAQ_OD product yields better agreement with ACAM NO_2. The low r^2-values may be related to the ACAM instrument random error, one of which is the use of unpolluted background spectra instead of reference spectra to process the data (Lamsal et al., 2017). In Figure 8a, we shade the points based on date. There were only six days in which valid OMI NO_2 spatially and temporally overlapped with the ACAM NO_2 data. In Figure 8b, we shade based on percentage coverage. Since the ACAM field of view is very small compared to OMI, pixel coverage from the ACAM would often only overlap a very small subset of the OMI pixel (median: 12 % of the OMI pixel). Since the ACAM is only measuring the portion of the tropospheric column below 8 km, there should be a consistent high bias in the OMI NO_2; instead there is a consistent low bias. This may be due to an artifact of the flight path of the UC-12 which preferentially sampled over the densest urban locations: OMI pixels are much larger in size and are capturing a more regional, and thus lower, value.

3.4.3 Comparison to the EPA NO_2 ground monitor network

The long-term EPA monitoring network provides surface observations outside the July 2011 timeframe. In Figure 9a, we compare mean NO_2* at each monitoring site to the two satellite products. All valid NO_2* data at each monitoring site over a 5-year (2008-2012) 2-month (June & July) period are averaged into a single point (up to 305 data entries) and matched to an average of satellite data over the same time period. The correlation between OMI_GMI and surface observations is $r^2 = 0.39$, while the correlation between OMI_CMAQ_OD and surface observations is $r^2 = 0.60$, a substantial improvement. This suggests that a high-resolution satellite product with improved AMFs, can detect surface NO_2 concentrations with more accuracy. As shown in Table 2, OMI_CMAQ without observational constraints performs almost as well ($r^2 = 0.55$); this is especially encouraging since comprehensive field measurements, such as those from DISCOVER-AQ, are limited in spatial and temporal scope.

3.5 OMI_CMAQ vs. CMAQ

We can now more fairly assess the NO_2 columns simulated by CMAQ using a high-resolution OMI NO_2 product. In Figure 10, we show a comparison between CMAQ and OMI_CMAQ_OD. Only model data within +/- 1 hour of and co-located with valid overpass data are shown in order to remove biases during cloudy days or days with invalid

data. We see a consistent model low bias in rural areas, and consistent model high bias in urban areas. Interestingly the high bias is larger in the immediate Baltimore metropolitan area compared to the D.C. metropolitan region.

We attribute the model low bias in rural regions to several shortcomings of this model simulation. This simulation did not include NO_x emissions from soils. Rasool et al. (2016) has shown soil NO_x emissions to be particularly important in the central United States, with a lesser role in the eastern United States. Excluding these emissions may have resulted in less NO_x being transported from upwind regions. This model simulation utilized CB05 gas-phase chemistry, which is known to underestimate the recycling of alkyl nitrates back to NO_2 (Hildebrandt-Ruiz and Yarwood, 2013; Canty et al., 2015). CB05e51 gas-phase chemistry, released in a newer version of CMAQ (https://www.airqualitymodeling.org/in-dex.php/CMAQ_v5.1_CB05_updates), better handles alkyl nitrates and employs faster recycling of short-lived alkyl nitrate species. Faster recycling of alkyl nitrates would yield higher NO_2 concentrations throughout the modeling domain. Travis et al. (2016) found that upper tropospheric NO_x is too low when compared to observations from aircraft during SEAC^{4}RS. This is possibly due to downward stratospheric transport, outflow from convection, or OH chemistry that is not characterized correctly by models. Lightning NO_x is still a very active area of research (Pickering et al., 2016). Although this model simulation did include lightning NO_x emissions, there is a possibility these emissions are underestimated.

We attribute the model high bias in urban regions within our domain to an overestimate of anthropogenic NO_x emissions (Anderson et al., 2014; Souri et al., 2016). This may be due to an improper allocation of area and mobile (on-road and off-road) source emissions which are spatially distributed based on population and number of cars respectively, or quite simply an overestimate of these sector emissions. Quantifying the uncertainty in MOVES, the mobile emissions software, is an active area of research.

3.6 Comparison of model to satellite and in situ observations

To further evaluate the model, we compare the model simulation to DISCOVER-AQ and EPA observations. In Figure 7b, we show a Pandora NO_2 comparison in the same manner as Figure 7a. In addition to showing CMAQ, we also show OMI_CMAQ_OD. We add the stratospheric VCD information from the OMI NO_2 Level 2 product to the CMAQ tropospheric columns to ensure a fair comparison. Both the model and new OMI NO_2 product have a slope close to unity indicating that both are able to match the variability in NO_2 columns. There is, however, a consistent low offset. This may indicate that the stratospheric VCD in the NASA Level 2 retrieval may be too low during this two-month timeframe. The r^2 of CMAQ is higher than OMI_CMAQ_OD. This is not particularly surprising because the resolution of the satellite is coarse, despite it being processed with new air mass factors.

In Figure 9b, we show a comparison between CMAQ, OMI_CMAQ_OD and ground monitors for June & July 2011. The r^2 between CMAQ and ground monitors is 0.70, while the correlation with the new satellite product is 0.73. The OMI_CMAQ_OD product has a better correlation with ground NO_2 monitors than the 1.33 km CMAQ simulation alone indicating that there is added utility in the satellite data.

4 Summary and conclusions

This study demonstrates the critical importance of using high-resolution a priori NO_2 shape factors to develop AMFs in and around metropolitan areas. We develop three new OMI NO_2 products: using high spatial resolution NO_2 profiles from a 1.33 km CMAQ model simulation (OMI_CMAQ), using CMAQ profiles constrained by in-situ observations (OMI_CMAQ_O), and applying model-derived spatial information (downscaling) to OMI_CMAQ_O (OMI_CMAQ_OD). When using high spatial resolution models to develop the AMF, the mean AMF in urban areas decreases by up to 50 % causing the tropospheric VCDs in urban areas to increase by up to a factor of two. This is because high-resolution models simulate larger concentrations near the surface in urban areas. In essence, we are reprocessing the satellite to look for NO_2 closer to the surface than in the original product. We believe this finding extends to other urban areas since coarse global models will consistently merge rural and urban pollution, and subsequently overestimate the AMF in city centers.

Another novel step in our re-processing technique is using in situ observations to enhance modeled NO_2 profile shapes. CMAQ NO_2 values in the Baltimore-Washington metropolitan region are generally too large within the boundary layer, too small in the mid-troposphere, and a factor of three too small in the uppermost troposphere. These particular biases may not be fully applicable to rural regions, since the DISCOVER-AQ field campaign was only focused in the urban corridor. As a result, our adjusted satellite product in rural regions may have higher uncertainty than urban areas. With that said, constraining model simulations to observations yields an improved satellite product over the non-constrained product when comparing to Pandora NO_2. Furthermore, by constraining to observations, we reduce the dependence on a priori emission inventories (e.g., NEI) used in model simulations, which can have deficiencies (Anderson et al., 2014; Souri et al., 2016; Travis et al., 2016). For example, in the constraint-based product, VCDs in Baltimore are 30 % lower than the OMI_CMAQ product. The tropospheric VCDs in rural Mid-Atlantic areas are 20 – 50 % lower than both the OMI_CMAQ and operational products. This is a particularly important finding because it means that the poor performance of CMAQ (or any model used for a satellite retrieval) will manifest itself in the retrieval. This will be a difficult challenge going forward, and emphasizes the need to use state-of-the science models for satellite retrievals.

Lastly, we apply a technique developed by Kim et al. (2016) to downscale OMI NO_2 data. This technique is especially valuable for pollutant exposure health studies, which require high-resolution long-term pollutant estimates. The downscaling procedure provides a higher spatial resolution snapshot of NO_2, while not altering the observed satellite pixel values. Instead, this technique re-allocates values across the pixel based on the variability within the high-resolution model. As a result, the new satellite product (OMI_CMAQ_OD) shows higher values in urban, polluted areas and lower values in rural, unpolluted areas than the operational OMI_GMI product. This new product better captures the urban-scale variability of NO_2 and has a much better correlation with ground monitors. A deficiency with this technique is that if a localized source, such as a power plant plume or wildfire, is not simulated at all by the model, then this error will be passed on to the product. Furthermore, if the area is affected by a mesoscale meteorological feature that is simulated incorrectly by the model, such as a thunderstorm, valley breeze,

or sea breeze, the model will be similarly deficient. Therefore, we do not recommend using the downscaling technique in areas where the emission inventory or meteorology is very uncertain.

We must clarify, however, that the results in this paper are only applicable to our region of interest. While we find that rural areas within our mid-Atlantic model domain now have tropospheric NO_2 columns which are 20 – 50 % lower than the operational product, we cannot conclude that this would be the same elsewhere. The "rural" locations within our model domain are situated in a particularly tricky spot because they are close, but not too close to major urban areas: a GMI simulation with a resolution of 1.25° × 1° (~110 × 110 km) will group rural areas into a grid cell also including a large city. Therefore a location that is 100's of kilometers from the nearest city and with spatial homogeneity may be simulated with consistency by GMI and therefore the operational OMI product may be an accurate representation of reality in these cases.

The refined OMI_CMAQ_OD product provides a better NO_2 column measurement when compared to Pandora column NO_2: the slope is near unity and the r^2 increases over the operational OMI NO_2 product. An important finding of this work is that using a high-resolution model, not the constraining to observations, provides the majority of the improvement, when comparing to ground monitors. This suggests that a high-resolution model with reasonable fidelity can be used anywhere in the world, and is not tied into an area in which a field experiment is located.

This technique can be used as a bridge until newer instruments such as TROPOMI are instituted. Future instruments will have increased spatial resolution, but comparison to OMI without using this technique may yield large differences around urban areas. At the same time, we demonstrate the importance of using high-resolution and high-fidelity model simulations for retrievals from future satellite missions. A combination of both increased satellite resolution and model resolution are needed in order to improve NO_2 satellite retrievals. We urge other community members to generate high-resolution OMI NO_2 data using this technique if it is to be used for small-scale (< 100 km length scale) studies as it provides a better alternative for urban areas than standard satellite products.

Acknowledgments

This publication was developed under Assistance Agreement No. RD835871 awarded by the U.S. Environmental Protection Agency to Yale University. It has not been formally reviewed by EPA. The views expressed in this document are solely those of the authors and do not necessarily reflect those of the Agency. EPA does not endorse any products or commercial services mentioned in this publication. We would like to thank two anonymous reviewers for their constructive comments in improving this work. We would like to thank Ron Cohen of UC-Berkeley and his research group for their observations of NO_2 from the P3-B aircraft during DISCOVER-AQ Maryland. We would also like to thank Jay Herman of UMBC and NASA Goddard Space Flight Center and his research group for their Pandora NO_2 measurements during this same time period. All data from DISCOVER-AQ Maryland can be downloaded freely from http://www-air.larc.nasa.gov/cgi-bin/ArcView/discover-aq.dc-2011. EPA NO_2* data was downloaded from the AQS Data Mart, and can be freely retrieved from:

https://aqs.epa.gov/aqsweb/documents/data_mart_wel-come.html. We would also like to thank Chinmay Satam formerly at the University of Maryland and now at Georgia Tech for preparation of the emissions in the CMAQ model simulation. We acknowledge the free use of NO_2 column data from the OMI sensor available at: https://disc.gsfc.nasa.gov/Aura/data-holdings/OMI/omno2_v003.shtml. Argonne National Laboratory is operated by UChicago Argonne, LLC, under contract no. DE-AC2-06CH11357 with the U.S. Department of Energy.

References

Acarreta, J. R., De Haan, J. F., and Stammes, P.: Cloud pressure retrieval using the O_2-O_2 absorption band at 477 nm, J. Geophys. Res., 109, D05204, 2004.

Allen, D. J., Pickering, K. E., Pinder, R. W., Henderson, B. H., Appel, K. W., and Prados, A.: Impact of lightning-NO on eastern United States photochemistry during the summer of 2006 as determined using the CMAQ model, Atmos. Chem. Phys., 12, 1737-1758, 2012.

Anderson, D. C., Loughner, C. P., Diskin, G., Weinheimer, A., Canty, T. P., Salawitch, R. J., Worden, H. M., Fried, A., Mikoviny, T., Wisthaler, A., and Dickerson, R. R.: Measured and modeled CO and NOy in DISCOVER-AQ: An evaluation of emissions and chemistry over the eastern US, Atmos. Environ., 96, 78-87, 2014.

Bechle, M. J., Millet, D. B., and Marshall, J. D.: National Spatiotemporal Exposure Surface for NO_2: Monthly Scaling of a Satellite-Derived Land-Use Regression, 2000–2010, Environ. Sci. & Tech., 49, 12297-12305, 2015.

Beirle, S., Boersma, K. F., Platt, U., Lawrence, M. G., and Wagner, T.: Megacity Emissions and Lifetimes of Nitrogen Oxides Probed from Space, Science, 333, 1737-1739, 2011.

Boersma, K. F., Eskes, H. J., and Brinksma, E. J.: Error analysis for tropospheric NO2 retrieval from space, J. Geophys. Res. Atmos., 109, 2004.

Boersma, K. F., Eskes, H. J., Veefkind, J. P., Brinksma, E. J., Van Der A, R. J., Sneep, M., Van Der Oord, G. H. J., Levelt, P. F., Stammes, P., and Gleason, J. F.: Near-real time retrieval of tropospheric NO_2 from OMI, Atmos. Chem. Phys., 7, 2103-2118, 2007.

Boersma, K. F., Jacob, D. J., Eskes, H. J., Pinder, R. W., and Wang, J.: Intercomparison of SCIAMACHY and OMI tropospheric NO_2 columns: Observing the diurnal evolution of chemistry and emissions from space, J. Geophys. Res. Atmos., 113, 2008a.

Boersma, K. F., Jacob, D. J., Bucsela, E. J., Perring, A. E., Dirksen, R., Yantosca, R. M., Park, R. J., Wenig, M. O., Bertram, T. H., and Cohen, R. C.: Validation of OMI tropospheric NO_2 observations during INTEX-B and application to constrain NOx emissions over the eastern United States and Mexico, Atmos. Environ., 42, 4480-4497, 2008b.

Boersma, K. F., Eskes, H. J., Dirksen, R. J., Veefkind, J. P., Stammes, P., Huijnen, V., Kleipool, Q. L., Sneep, M., Claas, J., and Leitão, J.: An improved tropospheric NO2 column retrieval algorithm for the Ozone Monitoring Instrument, Atmos. Meas. Tech., 4, 1905, 2011.

Boersma, K. F., Vinken, G. C. M., and Tournadre, J.: Ships going slow in reducing their NOx emissions: changes in 2005–2012 ship exhaust inferred from satellite measurements over Europe, Environ. Res. Lett., 10, 074007, 2015.

Bovensmann, H., Burrows, J. P., Buchwitz, M., Frerick, J., Noël, S., Rozanov, V. V., Chance, K. V., and Goede, A. P. H.: SCIAMACHY: Mission objectives and measurement modes, J. Atmos. Sci., 56, 127-150, 1999.

Bucsela, E. J., Celarier, E. A., Wenig, M. O., Gleason, J. F., Veefkind, J. P., Boersma, K. F., and Brinksma, E. J.: Algorithm for NO_2 Vertical Column Retrieval From the Ozone Monitoring Instrument, IEEE Transactions on Geoscience and Remote Sensing, 44, 1245-1258, 2006.

Bucsela, E., Krotkov, N., Celarier, E., Lamsal, L., Swartz, W., Bhartia, P., Boersma, K., Veefkind, J., Gleason, J., and Pickering, K.: A new algorithm for retrieving vertical column NO2 from nadir-viewing satellite instruments: applications to OMI, Atmos. Meas. Tech, 6, 1361-1407, 2013.

Burrows, J. P., Weber, M., Buchwitz, M., Rozanov, V., Ladstätter-Weißenmayer, A., Richter, A., DeBeek, R., Hoogen, R., Bramstedt, K., and Eichmann, K.-U.: The global ozone monitoring experiment (GOME): Mission concept and first scientific results, J. Atmos. Sci., 56, 151-175, 1999.

Canty, T. P., Hembeck, L., Vinciguerra, T. P., Anderson, D. C., Goldberg, D. L., Carpenter, S. F., Allen, D. J., Loughner, C. P., Salawitch, R. J., and Dickerson, R. R.: Ozone and NOx chemistry in the eastern US: evaluation of CMAQ/CB05 with satellite (OMI) data, Atmos. Chem. Phys., 15, 10965-10982, 2015.

Chen, D., Zhou, B., Beirle, S., Chen, L. M., and Wagner, T.: Tropospheric NO2 column densities deduced from zenith-sky DOAS measurements in Shanghai, China, and their application to satellite validation, Atmos. Chem. Phys., 9, 3641-3662, 2009.

Conrad, R.: Soil microorganisms as controllers of atmospheric trace gases (H_2, CO, CH_4, OCS, N_2O, and NO)., Microbiological reviews, 60, 609-640, 1996.

Crawford, J. H., Dickerson R. R., and Hains, J.: DISCOVER-AQ: Observations and early results, Environmental Manager, 8-15, 2014.

Curier, R. L., Kranenburg, R., Segers, A. J. S., Timmermans, R. M. A., and Schaap, M.: Synergistic use of OMI

NO_2 tropospheric columns and LOTOS–EUROS to evaluate the NOx emission trends across Europe, Remote Sensing of Environment, 149, 58-69, 2014.

Day, D. A., Wooldridge, P. J., Dillon, M. B., Thornton, J. A., and Cohen, R. C.: A thermal dissociation laser-induced fluorescence instrument for in situ detection of NO_2, peroxy nitrates, alkyl nitrates, and HNO_3, J. Geophys. Res. Atmos., 107, ARTN 4046, 2002.

de Foy, B., Lu, Z., and Streets, D. G.: Impacts of control strategies, the Great Recession and weekday variations on NO 2 columns above North American cities, Atmos. Environ., 138, 74-86, 2016a.

de Foy, B., Lu, Z., and Streets, D. G.: Satellite NO2 retrievals suggest China has exceeded its NOx reduction goals from the twelfth Five-Year Plan, Scientific Reports, 6, 2016b.

de Foy, B., Lu, Z., Streets, D. G., Lamsal, L. N., and Duncan, B. N.: Estimates of power plant NOx emissions and lifetimes from OMI NO_2 satellite retrievals, Atmos. Environ., 116, 1-11, 2015.

Duncan, B. N., Strahan, S. E., Yoshida, Y., Steenrod, S. D., and Livesey, N.: Model study of the cross-tropopause transport of biomass burning pollution, Atmos. Chem. Phys., 7, 3713-3736, 2007.

Duncan, B. N., Lamsal, L. N., Thompson, A. M., Yoshida, Y., Lu, Z., Streets, D. G., Hurwitz, M. M., and Pickering, K. E.: A space based, high resolution view of notable changes in urban NOx pollution around the world (2005–2014), J. Geophys. Res. Atmos., 121, 976-996, 2016.

Dunlea, E. J., Herndon, S. C., Nelson, D. D., Volkamer, R. M., San Martini, F., Sheehy, P. M., Zahniser, M. S., Shorter, J. H., Wormhoudt, J. C., and Lamb, B. K.: Evaluation of nitrogen dioxide chemiluminescence monitors in a polluted urban environment, Atmos. Chem. Phys., 7, 2691-2704, 2007.

EPA: AQS Data Mart, 2016. https://aqs.epa.gov/aqsweb/documents/data_mart_welcome.html

Flynn, C. M., Pickering, K. E., Crawford, J. H., Lamsal, L., Krotkov, N., Herman, J., Weinheimer, A., Chen, G., Liu, X., and Szykman, J.: Relationship between column-density and surface mixing ratio: Statistical analysis of O_3 and NO_2 data from the July 2011 Maryland DISCOVER-AQ mission, Atmos. Environ., 92, 429-441, 2014.

Flynn, C. M., Pickering, K. E., Crawford, J. H., Weinheimer, A., Diskin, G., Thornhill, K. L., Loughner, C., Lee, P., and Strode, S.: Variability of O_3 and NO_2 profile shapes during DISCOVER-AQ: Implications for satellite observations and comparisons to model-simulated profiles, Atmos. Environ., 147, 133-156, 2016.

Goldberg, D. L., Loughner, C. P., Tzortziou, M., Stehr, J. W., Pickering, K. E., Marufu, L. T., and Dickerson, R. R.: Higher surface ozone concentrations over the Chesapeake Bay than over the adjacent land: Observations and models from the DISCOVER-AQ and CBODAQ campaigns, Atmos. Environ., 84, 9-19, 2014.

Goldberg, D. L., Vinciguerra, T. P., Anderson, D. C., Hembeck, L., Canty, T. P., Ehrman, S. H., Martins, D. K., Stauffer, R. M., Thompson, A. M., Salawitch, R. J., and Dickerson, R. R.: CAMx Ozone Source Attribution in the Eastern United States using Guidance from Observations during DISCOVER AQ Maryland, Geophys. Res. Lett., 43, 2016.

Han, K. M., Lee, S., Chang, L. S., and Song, C. H.: A comparison study between CMAQ-simulated and OMI-retrieved NO_2 columns over East Asia for evaluation of NOx emission fluxes of INTEX-B, CAPSS, and REAS inventories, Atmos. Chem. Phys., 15, 1913-1938, 2015.

Herman, J., Cede, A., Spinei, E., Mount, G., Tzortziou, M., and Abuhassan, N.: NO_2 column amounts from ground-based Pandora and MFDOAS spectrometers using the direct-sun DOAS technique: Intercomparisons and application to OMI validation, J. Geophys. Res., 114, D13307, 2009.

Heue, K.-P., Wagner, T., Broccardo, S. P., Walter, D., Piketh, S. J., Ross, K. E., Beirle, S., and Platt, U.: Direct observation of two dimensional trace gas distributions with an airborne Imaging DOAS instrument, Atmos. Chem. Phys., 8, 6707-6717, 2008.

Hilboll, A., Richter, A., and Burrows, J. P.: Long-term changes of tropospheric NO_2 over megacities derived from multiple satellite instruments, Atmos. Chem. Phys., 13, 4145-4169, 2013.

Hildebrandt-Ruiz, L., and Yarwood, G.: Interactions between organic aersol and NOy: influence on oxidant production, 2013.

Hudman, R. C., Russell, A. R., Valin, L. C., and Cohen, R. C.: Interannual variability in soil nitric oxide emissions over the United States as viewed from space, Atmos. Chem. Phys., 10, 9943-9952, 2010.

Huijnen, V., Eskes, H. J., Poupkou, A., Elbern, H., Boersma, K. F., Foret, G., Sofiev, M., Valdebenito, A., Flemming, J., Stein, O., Gross, A., Robertson, L., D'Isidoro, M., Kioutsioukis, I., Friese, E., Amstrup, B., Bergstrom, R., Strunk, A., Vira, J., Zyryanov, D., Maurizi, A., Melas, D., Peuch, V.-H., and Zerefos, C.: Comparison of OMI NO_2 tropospheric columns with an ensemble of global and European regional air quality models, Atmos. Chem. Phys., 10, 3273-3296, doi:10.5194/acp-10-3273-2010, 2010.

Ialongo, I., Herman, J., Krotkov, N., Lamsal, L., Boersma, K. F., Hovila, J., and Tamminen, J.: Comparison of OMI NO_2 observations and their seasonal and weekly cycles with ground-based measurements in Helsinki, Atmos. Meas. Tech., 9, 5203, 2016.

Kim, H. C., Lee, P., Judd, L., Pan, L., and Lefer, B.: OMI NO_2 column densities over North American urban cities: the effect of satellite footprint resolution, Geosci. Mod. Dev., 9, 1111-1123, 2016.

Kleipool, Q. L., Dobber, M. R., de Haan, J. F., and Levelt, P. F.: Earth surface reflectance climatology from 3 years of OMI data, J. Geophys. Res, Atmos,, 113, 2008.

Kowalewski, M. G., and Janz, S. J.: Remote sensing capabilities of the airborne compact atmospheric mapper, Proc. SPIE 7452, 74520Q, 2009.

Krotkov, N. A., McLinden, C. A., Li, C., Lamsal, L. N., Celarier, E. A., Marchenko, S. V., Swartz, W. H., Bucsela, E. J., Joiner, J., and Duncan, B. N.: Aura OMI observations of regional SO_2 and NO_2 pollution changes from 2005 to 2014, Atmos. Chem. Phys., 16, 4605-4629, 2016.

Krotkov, N. A., Lamsal, L. N., Celarier, E. A., Swartz, W. H., Marchenko, S. V., Bucsela, E. J., Chan, K. L., and Wenig, M. O.: The version 3 OMI NO_2 standard product, Atmos. Meas. Tech. Discuss., in review, 2017.

Kuhlmann, G., Lam, Y. F., Cheung, H. M., Hartl, A., Fung, J. C. H., Chan, P. W., and Wenig, W. O.: Development of a custom OMI NO_2 data product for evaluating biases in a regional chemistry transport model, Atmos. Chem. Phys., 15, 5627-5644, 2015.

Lamsal, L. N., Martin, R. V., van Donkelaar, A., Steinbacher, M., Celarier, E. A., Bucsela, E., Dunlea, E. J., and Pinto, J. P.: Ground-level nitrogen dioxide concentrations inferred from the satellite-borne Ozone Monitoring Instrument, J. Geophys. Res., 113, D16308, 2008.

Lamsal, L. N., Krotkov, N. A., Celarier, E. A., Swartz, W. H., Pickering, K. E., Bucsela, E. J., Gleason, J. F., Martin, R. V., Philip, S., and Irie, H.: Evaluation of OMI operational standard NO_2 column retrievals using in situ and surface-based NO_2 observations, Atmos. Chem. Phys., 14, 11587-11609, 2014.

Lamsal, L. N., Duncan, B. N., Yoshida, Y., Krotkov, N. A., Pickering, K. E., Streets, D. G., and Lu, Z.: US NO_2 trends (2005 - 2013): EPA Air Quality System (AQS) data versus improved observations from the Ozone Monitoring Instrument (OMI), Atmos. Environ., 110, 130-143, 2015.

Lamsal, L. N., Janz, S. J., Krotkov, N. A., Pickering, K. E., Spurr, R. J. D., Kowalewski, M. G., Loughner, C. P., Crawford, J. H., Swartz, W. H., and Herman, J. R.: High-resolution NO_2 observations from the Airborne Compact Atmospheric Mapper: Retrieval and validation, J. Geophys. Res. Atmos., 122, 1953-1970, 2017.

Laughner, J. L., Zare, A., and Cohen, R. C.: Effects of daily meteorology on the interpretation of space-based remote sensing of NO_2, Atmos. Chem. Phys., 16, 15247-15264, 2016.

Lee, H. J., and Koutrakis, P.: Daily ambient NO_2 concentration predictions using satellite ozone monitoring instrument NO_2 data and land use regression, Environ. Sci. & Tech., 48, 2305-2311, 2014.

Levelt, P. F., Van den Oord, G. H. J., Dobber, M. R., Malkki, A., Visser, H., de Vries, J., Stammes, P., Lundell, J. O. V., and Saari, H.: The Ozone Monitoring Instrument, IEEE Trans. Geosci. Rem. Sens., 44, 1093-1101, 2006.

Liaskos, C. E., Allen, D. J., and Pickering, K. E.: Sensitivity of tropical tropospheric composition to lightning NOx production as determined by replay simulations with GEOS-5, J. Geophys. Res. Atmos., 2015.

Lin, J. T., Liu, M. Y., Xin, J. Y., Boersma, K. F., Spurr, R., Martin, R., and Zhang, Q.: Influence of aerosols and surface reflectance on satellite NO_2 retrieval: seasonal and spatial characteristics and implications for NOx emission constraints, Atmos. Chem. Phys, 15, 11217-11241, 2015.

Lorente, A., Boersma, K. F., Yu, H., Dörner, S., Hilboll, A., Richter, A., Liu, M., Lamsal, L. N., Barkley, M., and De Smedt, I.: Structural uncertainty in air mass factor calculation for NO 2 and HCHO satellite retrievals, Atmos. Meas. Tech., 10, 759, 2017.

Loughner, C. P., Tzortziou, M., Follette-Cook, M., Pickering, K. E., Goldberg, D., Satam, C., Weinheimer, A., Crawford, J. H., Knapp, D. J., and Montzka, D. D.: Impact of bay breeze circulations on surface air quality and boundary layer export, J. Appl. Meteorol. Climatol., 53, 1697-1713, 2014.

Lu, Z., and Streets, D. G.: Increase in NOx emissions from Indian thermal power plants during 1996–2010: unit-based inventories and multisatellite observations, Environ. Sci. & Tech., 46, 7463-7470, 2012.

Lu, Z., Streets, D. G., de Foy, B., Lamsal, L. N., Duncan, B. N., and Xing, J.: Emissions of nitrogen oxides from US urban areas: estimation from Ozone Monitoring Instrument retrievals for 2005–2014, Atmos. Chem. Phys., 15, 10367-10383, 2015.

Ma, J. Z., Beirle, S., Jin, J. L., Shaiganfar, R., Yan, P., and Wagner, T.: Tropospheric NO2 vertical column densities over Beijing: results of the first three years of ground-based MAX-DOAS measurements (2008–2011) and satellite validation, Atmos. Chem. Phys., 13, 1547-1567, 2013.

Martin, R. V., Chance, K., Jacob, D. J., Kurosu, T. P., Spurr, R. J. D., Bucsela, E., Gleason, J. F., Palmer, P. I., Bey, I., and Fiore, A. M.: An improved retrieval of tropospheric nitrogen dioxide from GOME, J. Geophys. Res. Atmos., 107, 2002.

Martin, R. V., Jacob, D. J., Chance, K., Kurosu, T. P., Palmer, P. I., and Evans, M. J.: Global inventory of nitrogen oxide emissions constrained by space-based observations of NO_2 columns, J. Geophys. Res. Atmos., 108, 2003.

McLinden, C. A., Fioletov, V., Krotkov, N. A., Li, C., Boersma, K. F., and Adams, C.: A Decade of Change in NO_2 and SO_2 over the Canadian Oil Sands As Seen from Space, Environ. Sci. & Tech., 50, 331-337, 2015.

Novotny, E. V., Bechle, M. J., and Millet, D. B., and Marshall, J. D.: National satellite-based land-use regression: NO_2 in the United States, Environ. Sci. & Tech., 45, 4407-4414, 2011.

Palmer, P. I., Jacob, D. J., Chance, K. V., Martin, R. V., Spurr, R. J. D., Kurosu, T., Bey, I., Yantosca, R. M., Fiore, A., and Li, Q.: Air mass factor formulation for spectroscopic measurements from satellites: Application to formaldehyde retrievals from the Global Ozone Monitoring Experiment, J. Geophys. Res., 106, 14539-14550, 2001.

Pickering, K. E., Bucsela, E., D, Ring, A., Holzworth, R., and Krotkov, N.: Estimates of lightning NOx production based on OMI NO_2 observations over the Gulf of Mexico, J. Geophys. Res. Atmos., 121, 8668-8691, 2016.

Platt, U.: Differential optical absorption spectroscopy (DOAS), Air monitoring by spectroscopic technique, 127, 27-84, 1994.

Pujadas, M., Núñez, L., and Lubrani, P.: Assessment of NO_2 satellite observations for en-route aircraft emissions detection, Remote Sensing of Environment, 115, 3298-3312, 2011.

Rasool, Q. Z., Zhang, R., Lash, B., and Cohan, D. S., Cooter, E. J., Bash, J. O., Lamsal, L. N.: Enhanced representation of soil NO emissions in the Community Multiscale Air Quality (CMAQ) model version 5.0. 2, Geosci. Mod. Dev., 9, 3177-3197, 2016.

Ridley, B. A., Dye, J. E., Walega, J. G., Zheng, J., Grahek, F. E., and Rison, W.: On the production of active nitrogen by thunderstorms over New Mexico, J. Geophys. Res. Atmos., 101, 20985-21005, 1996.

Russell, A. R., Perring, A. E., Valin, L. C., Bucsela, E. J., Browne, E. C., Wooldridge, P. J., and Cohen, R. C.: A high spatial resolution retrieval of NO_2 column densities from OMI: method and evaluation, Atmos. Chem. Phys., 11, 8543-8554, 2011.

Russell, A. R., Valin, L. C., and Cohen, R. C.: Trends in OMI NO_2 observations over the US: effects of emission control technology and the economic recession, Atmos. Chem. Phys., 12, 12197-12209, 2012.

Souri, A. H., Choi, Y., Jeon, W., Li, X., Pan, S., Diao, L., and Westenbarger, D. A.: Constraining NOx emissions using satellite NO_2 measurements during 2013 DISCOVER-AQ Texas campaign, Atmos. Environ., 131, 371-381, 2016.

Souri, A. H., Choi, Y., Jeon, W., Woo, J., Zhang, Q., and Kurokawa, J.: Remote sensing evidence of decadal changes in major tropospheric ozone precursors over East Asia J. Geophys. Res, Atmos., 2017.

Strahan, S. E., Duncan, B. N., and Hoor, P.: Observationally derived transport diagnostics for the lowermost stratosphere and their application to the GMI chemistry and transport model, Atmos. Chem. Phys., 7, 2435-2445, 2007.

Streets, D. G., Canty, T., Carmichael, G. R., de Foy, B., Dickerson, R. R., Duncan, B. N., Edwards, D. P., Haynes, J. A., Henze, D. K., Houyoux, M. R., Jacob, D. J., Krotkov, N. A., Lamsal, L. N., Liu, Y., Lu, Z., Martin, R. V., Pfister, G. G., Pinder R. W., Salawitch, R. J., Wecht, K. J.: Emissions estimation from satellite retrievals: A review of current capability, Atmos. Environ., 77, 1011-1042, 2013.

Strode, S. A., Rodriguez, J. M., Logan, J. A., Cooper, O. R., Witte, J. C., Lamsal, L. N., Damon, M., Van Aartsen, B., Steenrod, S. D., and Strahan, S. E.: Trends and variability in surface ozone over the United States, J. Geophys. Res. Atmos., 120, 9020-9042, 2015.

Travis, K. R., Jacob, D. J., Fisher, J. A., Kim, P. S., Marais, E. A., Zhu, L., Yu, K., Miller, C. C., Yantosca, R. M., and Sulprizio, M. P.: Why do models overestimate surface ozone in the Southeast United States, Atmos. Chem. Phys., 16, 13561-13577, 2016.

Val Martin, M., Honrath, R. E., Owen, R. C., Pfister, G., Fialho, P., and Barata, F.: Significant enhancements of nitrogen oxides, black carbon, and ozone in the North Atlantic lower free troposphere resulting from North American boreal wildfires, J. Geophys. Res. Atmos., 111, 2006.

van Donkelaar, A., Martin, R. V., Leaitch, R. W., Macdonald, A. M., Walker, T. W., Streets, D. G., Zhang, Q., Dunlea, E. J., Jimenez, J. L., and Dibb, J. E.: Analysis of aircraft and satellite measurements from the Intercontinental Chemical Transport Experiment (INTEX-B) to quantify long-range transport of East Asian sulfur to Canada, Atmos. Chem. Phys., 8, 2999-3014, 2008.

van Vuuren, D. P., Bouwman, L. F., Smith, S. J., and Dentener, F.: Global projections for anthropogenic reactive nitrogen emissions to the atmosphere: an assessment of scenarios in the scientific literature, Current Opinion in Environmental Sustainability, 3, 359-369, 2011.

Vandaele, A. C., Hermans, C., Simon, P. C., Carleer, M., Colin, R., Fally, S., Merienne, M.-F., Jenouvrier, A., and Coquart, B.: Measurements of the NO_2 absorption cross-section from 42 000 cm− 1 to 10 000 cm− 1 (238–1000 nm) at 220 K and 294 K, Journal of Quantitative Spectroscopy and Radiative Transfer, 59, 171-184, 1998.

Veefkind, J. P., Aben, I., McMullan, K., Förster, H., De Vries, J., Otter, G., Claas, J., Eskes, H. J., De Haan, J. F.,

and Kleipool, Q.: TROPOMI on the ESA Sentinel-5 Precursor: A GMES mission for global observations of the atmospheric composition for climate, air quality and ozone layer applications, Remote Sensing of Environment, 120, 70-83, 2012.

Verstraeten, W. W., Neu, J. L., Williams, J. E., Bowman, K. W., Worden, J. R., and Boersma, K. F.: Rapid increases in tropospheric ozone production and export from China, Nat. Geosci., 8, 690, 2015.

Vienneau, D., Hoogh, K. D., Bechle, M. J., Beelen, R., van Donkelaar, A., Martin, R. V., Millet, D. B., Hoek, G., and Marshall, J. D..: Western European land use regression incorporating satellite-and ground-based measurements of NO_2 and PM10, Environ. Sci. & Tech., 47, 13555-13564, 2013.

Vinken, G. C. M., Boersma, K. F., Maasakkers, J. D., Adon, M., and Martin, R. V.: Worldwide biogenic soil NOx emissions inferred from OMI NO_2 observations, Atmos. Chem. Phys., 14, 10363-10381, 2014a.

Vinken, G. C. M., Boersma, K. F., van Donkelaar, A., and Zhang, L.: Constraints on ship NOx emissions in Europe using GEOS-Chem and OMI satellite NO2 observations, Atmos. Chem. Phys., 14, 1353-1369, 2014b.

Young, M. T., Bechle, M. J., and Sampson, P. D., Szpiro, A. A., Marshall, J. D., Sheppard, L., and Kaufman, J. D.: Satellite-Based NO_2 and Model Validation in a National Prediction Model Based on Universal Kriging and Land-Use Regression, Environ. Sci. & Tech., 50, 3686-3694, 2016.

Zhang, L., Jacob, D. J., Boersma, K. F., Jaffe, D. A., Olson, J. R., Bowman, K. W., Worden, J. R., Thompson, A. M., Avery, M. A., Cohen, R. C., Dibb, J. E., Flock, F. M., Fuelberg, H. E., Huey, L. G., McMillan, W. W., Singh, H. B., and Weinheimer, A. J.: Transpacific transport of ozone pollution and the effect of recent Asian emission increases on air quality in North America: an integrated analysis using satellite, aircraft, ozonesonde, and surface observations, Atmos. Chem. Phys., 8, 6117-6136, 2008.

Zoogman, P., Liu, X., Suleiman, R. M., Pennington, W. F., Flittner, D. E., Al-Saadi, J. A., Hilton, B. B., Nicks, D. K., Newchurch, M. J., and Carr, J. L.: Tropospheric emissions: monitoring of pollution (TEMPO), Journal of Quantitative Spectroscopy and Radiative Transfer, 186, 17-39, 2017.

Figures

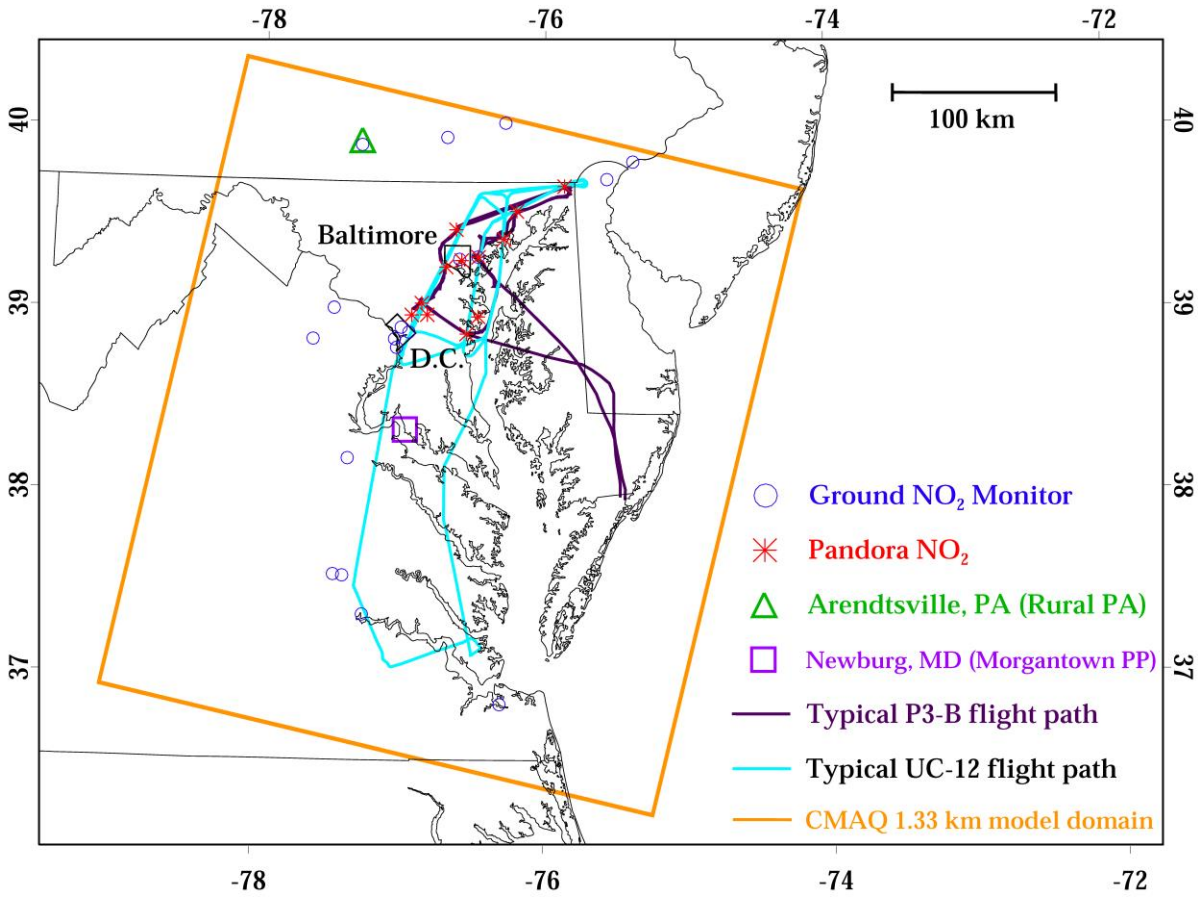

Figure 1. The Mid-Atlantic United States: the area of interest for this research project. Model domain and observation locations are depicted. There are eighteen EPA chemiluminescence NO_2 monitors and twelve Pandora NO_2 measurement sites.

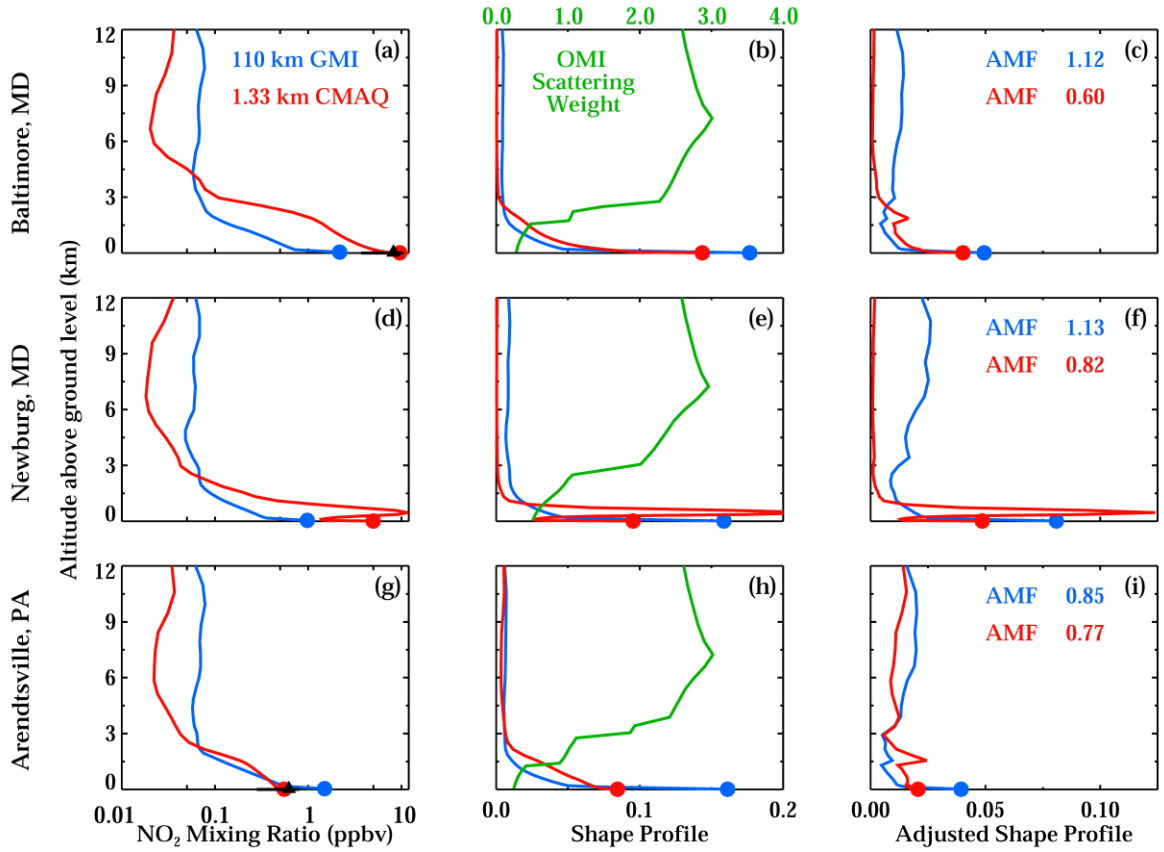

Figure 2. **(a, d, g)** Mean 2 PM local time June and July 2011 NO_2 mixing ratio as a function of altitude from a GMI (1.25° × 1°; ~110 ×110 km) model simulation and CMAQ (1.33 × 1.33 km) model simulation for three locations: **(a)** downtown Baltimore, **(d)** Morgantown power plant in Newburg, MD and **(g)** Arendtsville in rural Pennsylvania. Black triangles with error bars as discussed in the text represent co-located surface observations from the EPA monitoring network. **(b, e, h)** NO_2 shape profiles (partial NO_2 columns divided by total NO_2 column) as function of altitude for the same timeframe and locations; green line denotes co-located OMI scattering weight. **(c, f, i)** "Adjusted" shape profiles, partial NO_2 columns divided by total NO_2 columns multiplied by OMI scattering weight, as function of altitude for the same timeframe and locations.

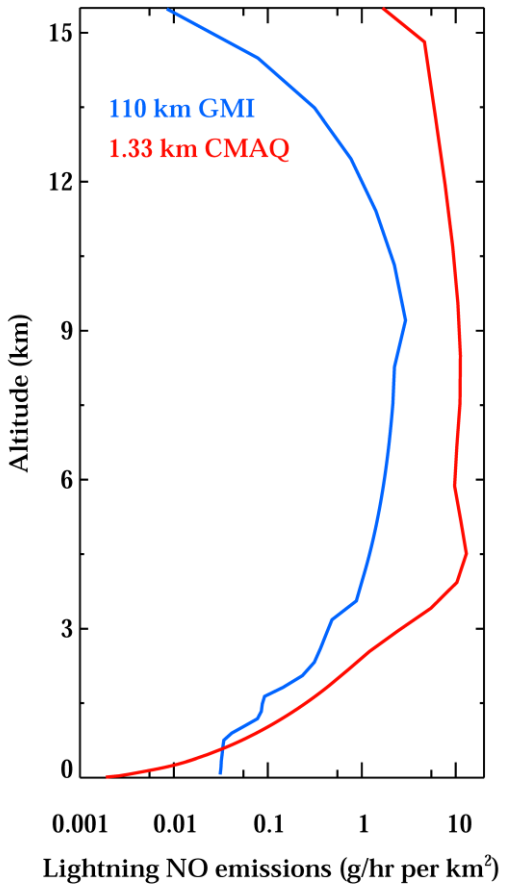

Figure 3. Mean June and July 2011 lightning NO emissions as a function of altitude from the GMI (1.25° × 1°; ~110 ×110 km) and CMAQ (1.33 × 1.33 km) model simulations.

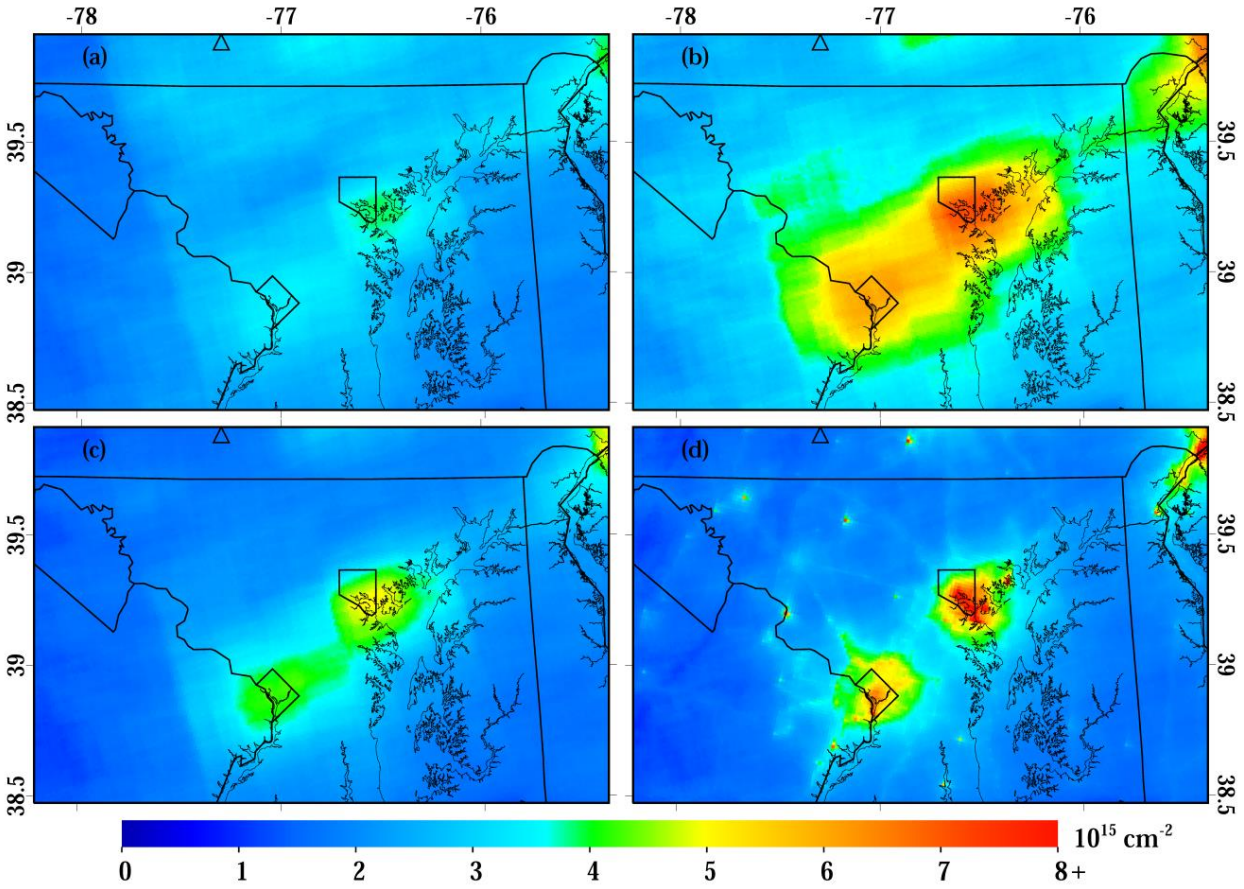

Figure 4. Oversampled OMI NO_2 tropospheric columns at 1.33 km resolution in the Baltimore-Washington metropolitan area for June & July 2008 – 2012 (2 months × 5 years; 10 months total). **(a)** The NASA version 3.0 operational OMI NO_2 product using GMI NO_2 shape profiles (OMI_GMI). **(b)** OMI NO_2 using CMAQ a priori NO_2 shape profiles (OMI_CMAQ). **(c)** OMI NO_2 using CMAQ a priori NO_2 shape profiles constrained by observations (OMI_CMAQ _O). **(d)** OMI NO_2 using CMAQ a priori NO_2 shape profiles constrained by observations and spatial weighting downscaling kernels (OMI_CMAQ_OD). In all plots, Arendtsville, PA is denoted by the triangle in the top left corner.

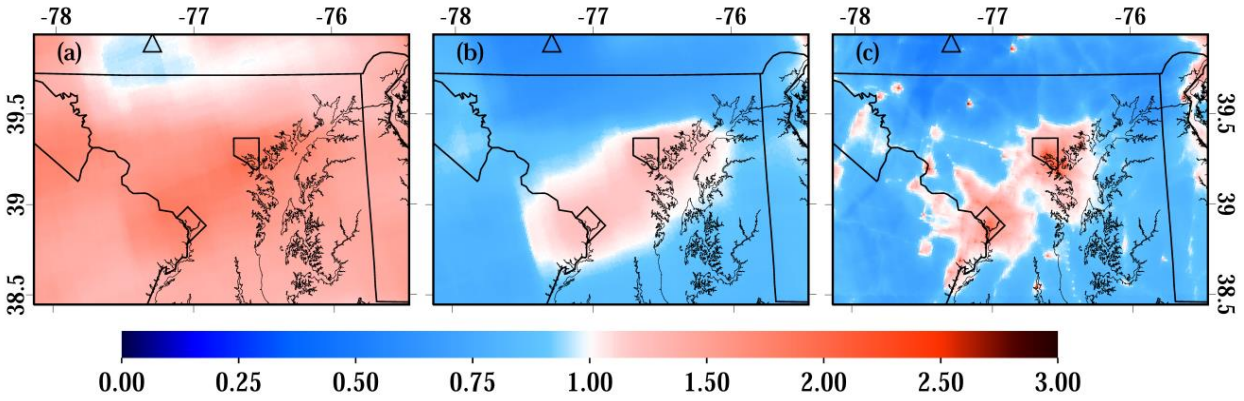

Figure 5. Ratio between the three OMI_CMAQ tropospheric NO_2 retrievals and the operational NASA v3.0 OMI tropospheric NO_2 retrieval for June & July 2008 – 2012 (2 months × 5 years; 10 months total). **(a)** OMI_CMAQ / OMI_GMI. **(b)** OMI_CMAQ_O/ OMI_GMI. **(c)** OMI_CMAQ_OD/ OMI_GMI.

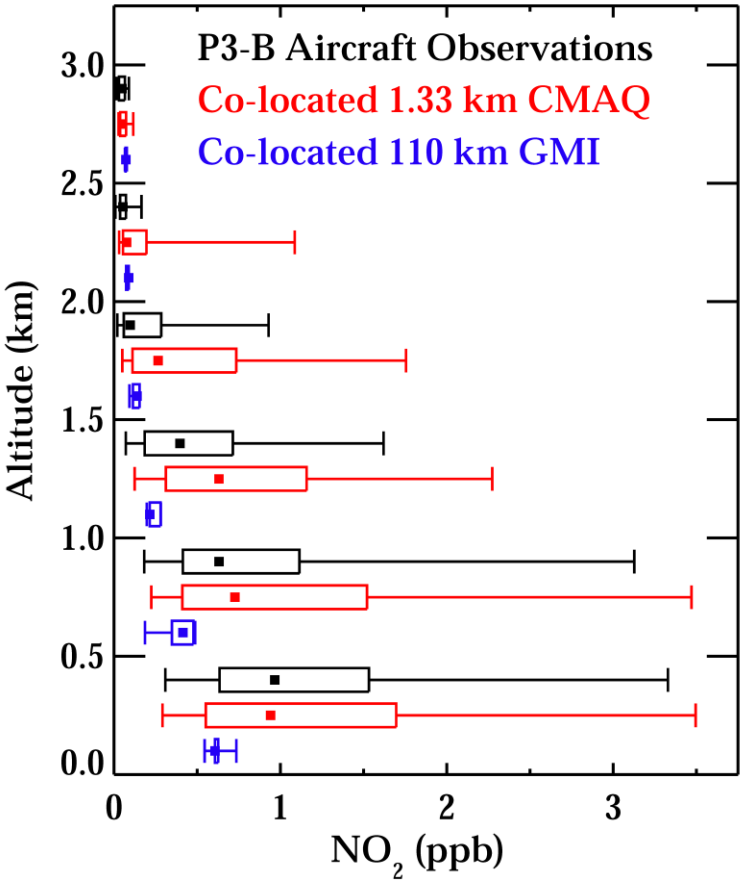

Figure 6. Vertical profiles of NO_2 binned in 500 m intervals (0 – 0.5 km, 0.5 – 1km, etc.) showing the 5th, 25th, 50th, 75th, and 95th percentiles within ± 2 hours of the OMI overpass time. **(Black)** One minute averaged data from the P3-B aircraft during July 2011 DISCOVER-AQ Maryland. **(Red)** Model output from CMAQ matched spatially and temporally to the P3-B measurements at 1 min intervals. **(Blue)** July 2011 monthly mean model output from GMI matched spatially to the P3-B measurements at 1 min intervals. In all cases, the squares indicate the median values.

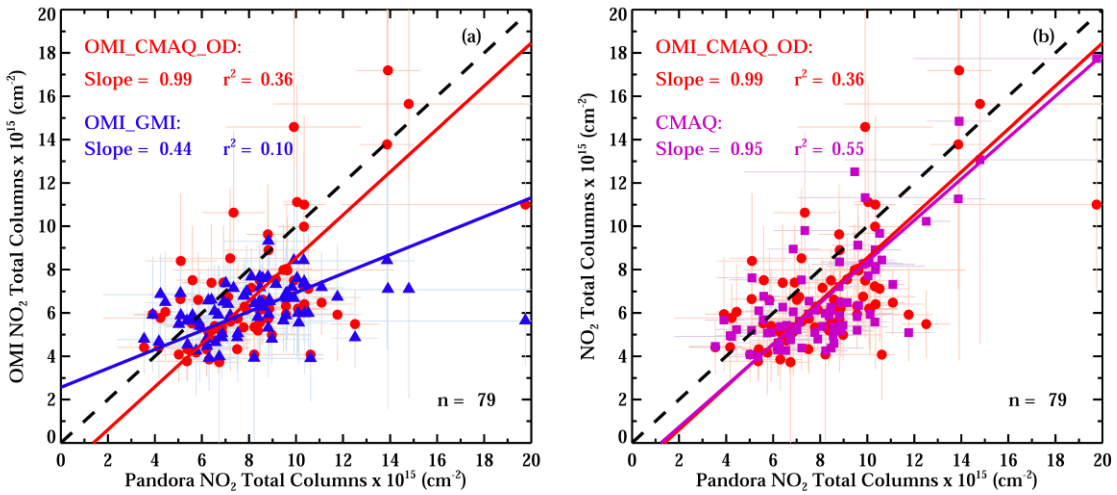

Figure 7. (a) Total column NO_2 OMI_GMI and OMI_CMAQ_OD versus co-located spatially and temporally Pandora NO_2 total column measurements within ± 1 hour of a valid satellite overpass during July 2011. (b) Same but now showing CMAQ instead of OMI_GMI; the stratospheric vertical column from NASA Level 2 product has been added to CMAQ to ensure a fair comparison. Error bars on both plots represent ± one standard deviation away from the mean**.**

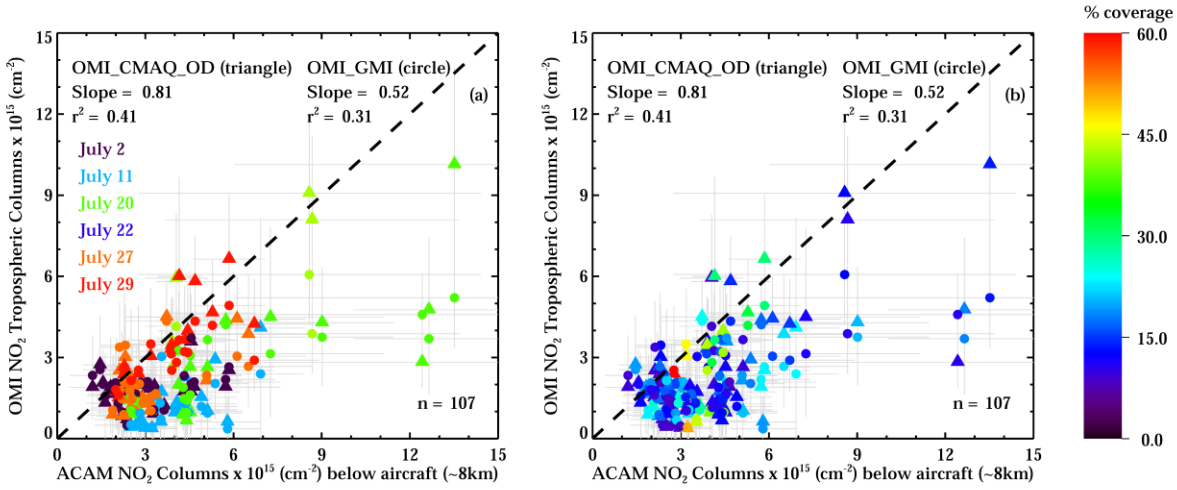

Figure 8. Tropospheric column NO_2 OMI_GMI and OMI_CMAQ_OD versus co-located spatially and temporally matched ACAM NO_2 column measurements within ± 1 hour of a valid satellite overpass during July 2011. **(a)** Color-coded based on date. **(b)** Color-coded based on percent coverage. Error bars on both plots represent ± one standard deviation away from the mean**.**

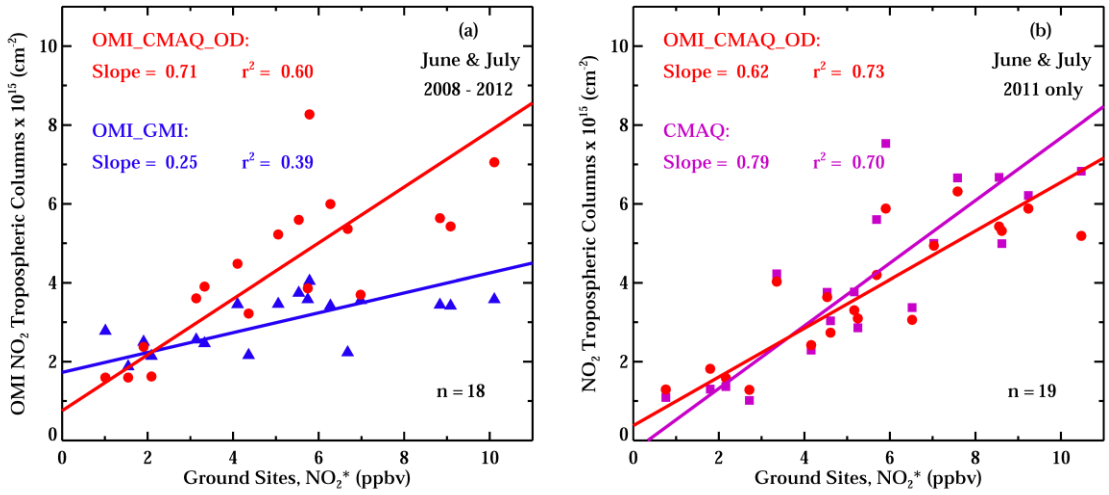

Figure 9. (a) Tropospheric column NO_2 OMI_GMI and OMI_CMAQ_OD versus co-located ground NO_2* chemiluminescence measurements within ± 2 hours of a valid satellite overpass during June & July 2008 through 2012; all ~300 daily ground monitor values are merged into a mean single value and compared to the satellite mean over the same corresponding time period. **(b)** Same as (a) but now comparing CMAQ and OMI_CMAQ_OD for June & July 2011 only.

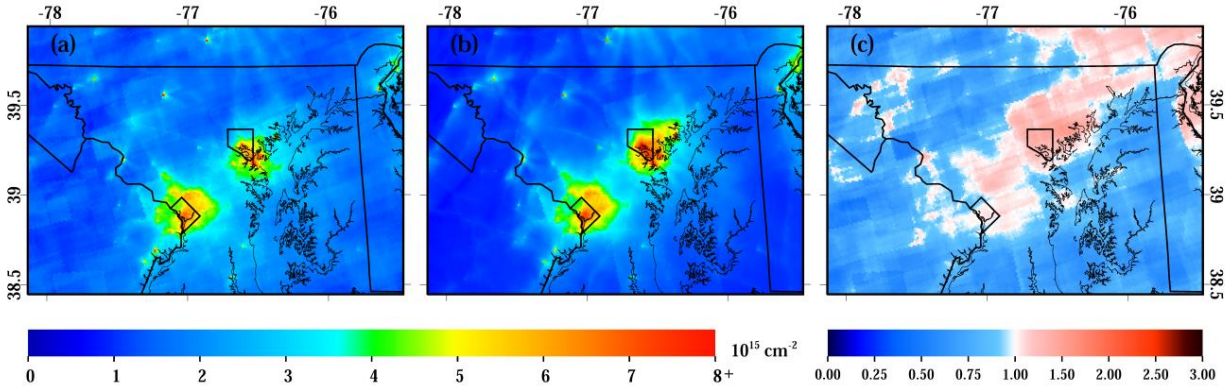

Figure 10. Oversampled tropospheric column NO_2 at 1.33 km in the Baltimore-Washington metropolitan area for June & July 2011 only. **(a)** OMI_CMAQ_OD. **(b)** CMAQ NO_2 corresponding to valid overpass times. **(c)** Ratio between the two plots CMAQ / OMI_CMAQ_OD.

Table 1. Summary of the current OMI NO_2 retrievals in the literature.

	NASA OMNO2 v3	DOMINO v2	BeHR NO_2	POMINO	HKOMI NO_2	This study
CTM	GMI Global 1° × 1.25°	TM4 Global 2° × 3°	WRF-Chem U.S. 12 × 12 km	GEOS-Chem China 0.667° × 0.5°	WRF-CMAQ PRD China 3 × 3 km	WRF-CMAQ East U.S. 1.33 × 1.33 km
RTM	TOMRAD	DAK	TOMRAD	LIDORT v3.6	SCIATRAN	TOMRAD
A priori NO_2 profile	Monthly mean profiles	Monthly mean profiles	Daily profiles when it exists. Monthly mean profiles elsewhere.	Monthly mean profiles	Daily profiles	Daily profiles when it exists. Monthly mean profiles elsewhere. All profiles constrained to aircraft observations.
Surface pressure	MERRA downscaled to 90 arcsec DEM	TM4 downscaled to 3 × 3 km	WRF downscaled to 1 × 1 km using GLOBE	GEOS-5 0.667° × 0.5°	WRF 3 × 3 km	WRF 1.33 × 1.33 km
Surface albedo	OMI LER climatology 0.5° × 0.5° taken from Kleipool et al., 2008	OMI LER climatology 0.5° × 0.5° taken from Kleipool et al., 2008	MODIS black-sky albedo MCD43C2 at 0.05° × 0.05°	Over land: MODIS BRDF MCD43C2 at 0.05° × 0.05° Over ocean: OMI LER taken from Kleipool et al., 2008	MODIS MCD43C2 at 0.01° × 0.01°	OMI LER climatology 0.5° × 0.5° taken from Kleipool et al., 2008
Aerosol correction	Implicitly corrected through cloud products	Implicitly corrected through cloud products	Implicitly corrected through cloud products	Explicit treatment of aerosols	Correction for the aerosol effect	Implicitly corrected through cloud products

Table 2. Slope and r^2 for all four OMI satellite products compared to Pandora NO_2 from July 2011 and EPA ground monitor NO_2* observations from June & July 2008 – 2012. Pandora NO_2 is compared to the OMI NO_2 total column products, while the EPA ground monitors are compared to OMI NO_2 tropospheric column products. Figures 7a and 9a show values for OMI_GMI and OMI_CMAQ_OD only.

	Pandora NO_2		EPA NO_2*	
	Slope	r^2	Slope	r^2
OMI_GMI	0.44	0.10	0.25	0.39
OMI_CMAQ	1.23	0.12	0.54	0.55
OMI_CMAQ_O	0.64	0.18	0.41	0.57
OMI_CMAQ_OD	0.99	0.36	0.71	0.60